THE GEOLOGICAL SOCIETY OF AMERICA®

Time scale for the development of thickened crust in the Cretaceous North Cascades magmatic arc, Washington, and relationship to Cretaceous flare-up magmatism

Erin K. Shea[1,†], Jonathan S. Miller[2], Robert B. Miller[2], Christine F. Chan[3,4], Adam J.R. Kent[3], John M. Hanchar[5], Kelly Dustin[2], and Scott Elkins[2]

[1]DEPARTMENT OF EARTH, ATMOSPHERIC, AND PLANETARY SCIENCES, MASSACHUSETTS INSTITUTE OF TECHNOLOGY, CAMBRIDGE, MASSACHUSETTS 02139, USA
[2]DEPARTMENT OF GEOLOGY, SAN JOSE STATE UNIVERSITY, SAN JOSE, CALIFORNIA 95112, USA
[3]COLLEGE OF EARTH, OCEAN, AND ATMOSPHERIC SCIENCES, OREGON STATE UNIVERSITY, CORVALLIS, OREGON 97331, USA
[4]DEPARTMENT OF GEOLOGY, UNIVERSITY OF KANSAS, LAWRENCE, KANSAS 66045, USA
[5]DEPARTMENT OF EARTH SCIENCES, MEMORIAL UNIVERSITY OF NEWFOUNDLAND, ST. JOHN'S, NEWFOUNDLAND A1B 3X5, CANADA

ABSTRACT

Heavy rare earth element (HREE)–depleted trace-element patterns are a relatively common feature of granitoids within mature Cordilleran continental margin arcs (e.g., Sierra Nevada batholith, Coast Mountains batholith, North Cascades, Peninsular Ranges batholith). This depletion is commonly interpreted to indicate the presence of garnet during granitoid melt formation, which requires thick arc crust (>40 km) to achieve the necessary pressure conditions to stabilize garnet in the lower crust. This work focused on understanding the evolution of thickened crust in an ancient continental arc using whole-rock geochemical data, high-precision chemical abrasion–isotope dilution–thermal ionization mass spectrometry (CA-ID-TIMS) U-Pb zircon geochronology, and in situ zircon Hf and O isotopic data from three contemporaneous Cretaceous plutons in the North Cascades of Washington State, USA.

New data show that, over time, magmas from three North Cascades plutons became more felsic and more HREE-depleted but lacked a significant change in zircon $\delta^{18}O$. The gradual depletion in HREEs through time is interpreted as evidence for a progressively thickening crust in the North Cascades arc that only became thick enough to stabilize garnet between 90 Ma and 87 Ma. This time frame also coincides with the end of a major period of contraction and plutonism in the region, suggesting a link between thick crust and the end of a major magmatic flare-up. The absence of appreciable change in zircon $\delta^{18}O$ values during this time suggests that thickening may have been the result of crustal shortening within the arc, causing migration of the magma source region to below the garnet stability threshold.

LITHOSPHERE; v. 10; no. 6; p. 708–722; GSA Data Repository Item 2018356 | Published online 11 October 2018 https://doi.org/10.1130/L1001.1

INTRODUCTION

Many arc rocks show strongly depleted heavy rare earth element (HREE) trace-element patterns, which are often interpreted to indicate the presence of garnet ± amphibole during melt generation. Garnet may be a residue left behind following partial melting in the deep crust (e.g., Kelemen et al., 2003; Saleeby et al., 2003; Lee et al., 2006), or it may form during fractional crystallization (Green, 1972; Green and Ringwood, 1968; Müntener et al., 2001; Alonso-Perez and Müntener, 2009). Both of these processes require the lower crust to reach sufficiently high-pressure conditions for garnet to be stable during magma genesis (~1.2 GPa; Alonso-Perez and Müntener, 2009). The nature and timing of the growth of garnet in the lower crust of arcs are still relatively poorly understood but have been studied in the Andean arc (Mamani et al., 2010), where a correlation was found between the development of a garnet signature and crustal thickening. Additional work by Chapman et al. (2015), Chiaradia (2015), and Profeta et al. (2015) found distinct correlations between geochemical signatures (elevated Sr/Y and La/Yb_N) and crustal thickness; however, the age resolution of crustal thickening was relatively coarse. The relative timing and rates of crustal thickening are important to establish because they provide constraints on mechanisms of crustal thickening (Karlstrom et al., 2014; Chin et al., 2015). This timing is particularly relevant in the North America Cordillera, where crustal thickening has been invoked as the primary trigger for the Cretaceous magmatic flare-ups (Ducea, 2001; DeCelles et al., 2009; Girardi et al., 2012).

Understanding the triggering mechanisms of flare-up magmatism requires a fuller picture of the timing of physical and chemical changes that occur within an arc as the crust thickens, which in turn requires detailed geochemical and isotopic work on sufficiently well-dated igneous rocks. Several studies of exposed and tilted oceanic arcs suggest that garnet as a fractionating phase in the lower crust dominates the HREE budget, while amphibole exerts primary control on the middle rare earth elements (MREEs; Greene et al., 2006; Jagoutz et al., 2009). These minerals, along with plagioclase, affect the rare earth element (REE) profiles for magmas produced in, or interacting with, the deep crust. Although ideal for focused research, such exposures of complete arc sections are rare. Structural, geochronologic, and geochemical studies of arc granitoids are often limited to a single crustal level within an arc magma system, providing an incomplete window into arc processes. In particular, exposures

†Corresponding author e-mail: ekshea@alum.mit.edu. Present address: Bishop, California, USA

of deep crustal (i.e., >25 km) plutons are uncommon, making it difficult to understand the connection (if any) between deep and shallow crustal magmatism (e.g., Miller and Snoke, 2009, and references therein). In general, plutonic systems are not well dated, typically relying on one or two samples to represent hundreds or thousands of square kilometers. This temporal aspect is critical to establishing the rate of crustal thickening and the changing composition of the lower crust, which are, in turn, critical to understanding the detailed petrogenesis of arc magmas, and especially the triggers for magmatic flare-ups in continental arcs.

The North Cascades of Washington State offer an exceptional field laboratory in which to study magmatism in an ancient continental arc because exposures of igneous rocks extend from the deep crust (>30 km) to the surface. These exposures offer unique snapshots into the workings of a classic Cordilleran magmatic arc at various depths. Several Late Cretaceous plutons in the North Cascades, which intruded during a magmatic flare-up and represent different crustal levels, have been very well dated using isotope dilution–thermal ionization mass spectrometry (ID-TIMS) U-Pb zircon geochronology (Matzel et al., 2006) and chemical abrasion–isotope dilution–thermal ionization mass spectrometry (CA-ID-TIMS; Shea, 2014; Shea et al., 2016; Chan et al., 2017). The high-precision geochronology from these plutons provides a temporal link for new geochemical and isotopic data and published structural information. CA-ID-TIMS is commonly considered the "gold standard" for geochronology and regularly achieves precisions of <0.1%. Here, we used high-precision geochronology along with geochemical and isotopic data to investigate the time scale for the development of a garnet-bearing lower crust in a Cretaceous continental arc near the end of a magmatic flare-up.

GEOLOGIC SETTING

The crystalline core of the North Cascades (Cascades core) is located at the southern end of the 1500-km-long Coast Plutonic Complex, which stretches from southeast Alaska to northern Washington (Rubin et al., 1990). The core is bounded by the Eocene Straight Creek fault to the west, the Late Cretaceous(?)–Eocene Ross Lake fault zone (composed of the Hozameen, Foggy Dew, and Ross Lake faults, and the Gabriel Peak fault zone) to the east, and the Cretaceous Windy Pass thrust to the south (Fig. 1; Misch, 1966; Miller, 1985). Early Cretaceous magmatism in the North Cascades region occurred largely to the east of the Cascades core in the Okanogan Range batholith (Hurlow and Nelson, 1993) and in the Chelan Complex, an assemblage of deep-crustal arc rocks with uncertain relation to younger magmatism in the Cascades core (Hopson and Mattinson, 1994; Dessimoz et al., 2012). The Cascades core records evidence for mid-Cretaceous crustal shortening, metamorphism, and plutonism followed by Eocene transtension and magmatism (Misch, 1966; Tabor et al., 1989; Haugerud et al., 1991; Miller et al., 2009, 2016; Eddy et al., 2016). These two periods represent episodes of significant magmatic additions to the Cascades core (magmatic flare-ups), when large amounts of new igneous material were added to the region (Miller et al., 2009; Paterson et al., 2011).

This study focused on three contemporaneous Cretaceous plutons in the Cascades core that were intruded during the mid-Cretaceous (96–89 Ma) magmatic flare-up: (1) the shallow-crustal Black Peak intrusive complex, (2) the mid-crustal Seven-Fingered Jack pluton, and (3) the deep-crustal Tenpeak pluton (Fig. 1). These plutons comprise a variety of shapes, from thinly sheeted to broadly elliptical (Miller et al., 2009), and were generally intruded into previously accreted oceanic and arc terranes (Tabor et al., 1989). The plutons were intruded at a range of paleodepths (<5 km to >35 km; Brown and Walker, 1993; Dawes, 1993; Miller and Paterson, 2001; Miller et al., 2009), offering the ability to investigate contemporaneous magmatism at different crustal levels.

Geology of the Black Peak Intrusive Complex

The Black Peak intrusive complex (Shea et al., 2016) is an elliptical-shaped body emplaced along the eastern edge of the Cascades core (Fig. 1). Two dextral faults form the eastern and western margins of the region: the North Creek fault on the east and the Gabriel Peak fault zone on the west, both of which are considered part of the Ross Lake fault zone (Fig. 2A; Miller and Bowring, 1990; Miller, 1994). Al-in-hornblende barometry on samples from the Black Peak intrusive complex indicates that the eastern margin of the complex crystallized at 0.1–0.3 GPa, which is compatible with the low metamorphic grade of host rocks on the east into which the complex intrudes (Fig. 1; D.L. Whitney and R.B. Miller, personal data from four samples).

Rocks of the Black Peak intrusive complex are dominated by tonalite and granodiorite, but diorite, gabbro, and granite are also present (Adams, 1964; Miller, 1994). Intrusive relationships and geochronology suggest a temporal progression from older mafic intrusions to younger felsic intrusions (Adams, 1964; Dragovich et al., 1997; Shea et al., 2016). The Black Peak intrusive complex is subdivided into four units based on textural and compositional characteristics. Listed from oldest to youngest, along with their zircon U-Pb CA-TIMS dates and 2σ analytical uncertainty, these units are the Crescent Mountain unit (91.755 ± 0.040 Ma to 91.18 ± 0.12 Ma), the Stiletto Mountain unit (90.345 ± 0.030 Ma to 88.81 ± 0.30 Ma), the Reynolds Peak unit (88.467 ± 0.031 Ma to 87.765 ± 0.072 Ma), and the War Creek unit (87.474 ± 0.052 Ma to 86.862 ± 0.062 Ma; Fig. 2A; Shea et al., 2016). Isotopic data from the Black Peak intrusive complex (Matzel et al., 2008; Shea et al., 2016) have a very limited range: $\varepsilon_{Nd(t)}$ whole-rock values are between +5.14 and +6.3 and zircon $\delta^{18}O$ values are between 6‰ and 7‰. Both isotopic data sets indicate contributions from isotopically juvenile sources such as subarc asthenospheric mantle and/or isotopically immature arc crust (e.g., the Napeequa/Twisp Valley schist, metamorphosed Methow basin sediments; Shea et al., 2016).

Geology of the Seven-Fingered Jack Pluton

The Seven-Fingered Jack pluton is an elongate intrusion emplaced east of the Entiat fault (Figs. 1 and 2B). The pluton intrudes the Napeequa unit (Napeequa schist of Cater and Crowder, 1967), which is in part Triassic in age (Sauer et al., 2017), and the Triassic Dumbell orthogneiss on its western margin (Fig. 2B; Cater and Crowder, 1967; Cater and Wright, 1967; Tabor et al., 1989). On its eastern margin, the Seven-Fingered Jack pluton intrudes the Dumbell orthogneiss and Triassic Holden assemblage (Fig. 2B; Cater and Crowder, 1967; Cater and Wright, 1967; Tabor et al., 1989). The southern margin of the Seven-Fingered Jack pluton is intruded by the Entiat pluton along a poorly mapped contact (Fig. 2B). Al-in-hornblende barometry from several locations in the Seven-Fingered Jack pluton suggests pressures of 0.6–0.7 GPa, indicating crystallization depths of 20–25 km (Dawes, 1993). These data are consistent with pressures of 0.7 GPa (Garnet-Aluminosilicate-Silica-Plagioclase [GASP]) at 650 °C from a sample of metapelitic Napeequa unit collected adjacent to the Seven-Fingered Jack pluton (Valley et al., 2003). Extensive field work by Paterson and Miller (1998) and Miller and Paterson (2001) indicated that the Seven-Fingered Jack pluton is composed of multiple sheets of compositionally variable rock.

The Seven-Fingered Jack pluton is divided into three units, all of which are dominated by tonalite (Fig. 2B; Miller and Paterson, 2001; Matzel, 2004; Shea, 2014): Blue Creek unit (ca. 91.7 Ma to 90.5 Ma), the Cougar Mountain unit (ca. 90 Ma), and the Whistling Pig unit (ca. 88 Ma). Directly east of the Seven-Fingered Jack pluton, there is the Kelly Mountain pluton (ca. 78 Ma), an assemblage of tonalite, diorite, gabbro,

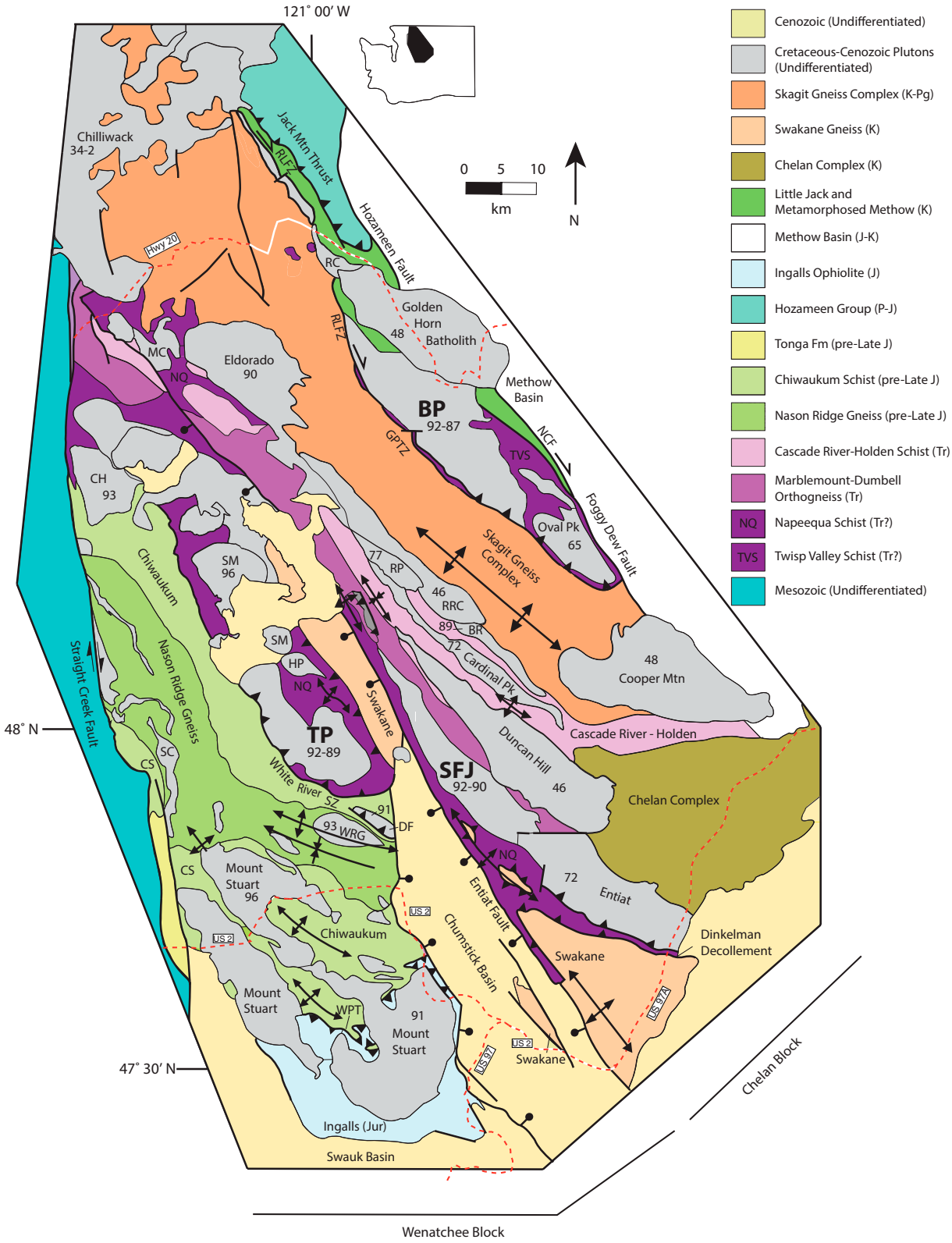

Figure 1. Crystalline core of the North Cascades. Numbers in plutons are crystallization ages. BP—Black Peak intrusive complex; BR—Bearcat Ridge orthogneiss; CH—Chaval pluton; CS—Chiwaukum schist; DF—Dirtyface pluton; GPTZ—Gabriel Peak tectonic zone; HP—High Pass pluton; MC—Marble Creek pluton; NCF—North Creek fault; NQ—Napeequa unit; RC—Ruby Creek plutonic belt; RRC—Railroad Creek pluton; RLF—Ross Lake fault; RLFZ—Ross Lake fault zone; RP—Riddle Peaks pluton; SC—Sloan Creek plutons; SFJ—Seven-Fingered Jack pluton; SM—Sulfur Mountain pluton; TP—Tenpeak pluton; TVS—Twisp Valley schist; WPT—Windy Pass thrust; WRG—Wenatchee Ridge gneiss. Regional fold traces and major highways are shown. Time periods: C—Cenozoic; J/Jur—Jurassic; K—Cretaceous; P—Permian; Pg—Paleogene; Tr—Triassic.

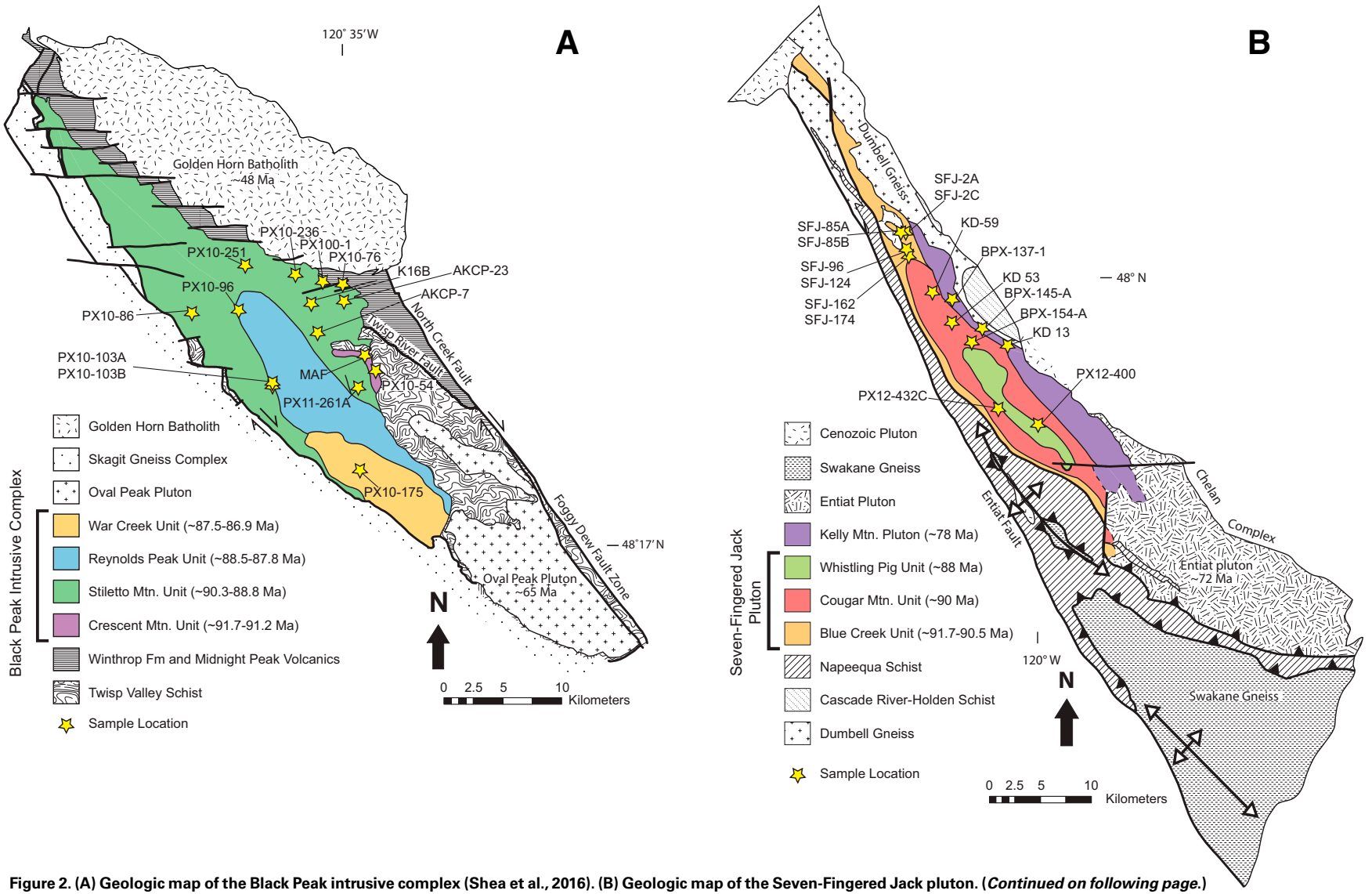

Figure 2. (A) Geologic map of the Black Peak intrusive complex (Shea et al., 2016). (B) Geologic map of the Seven-Fingered Jack pluton. (*Continued on following page.*)

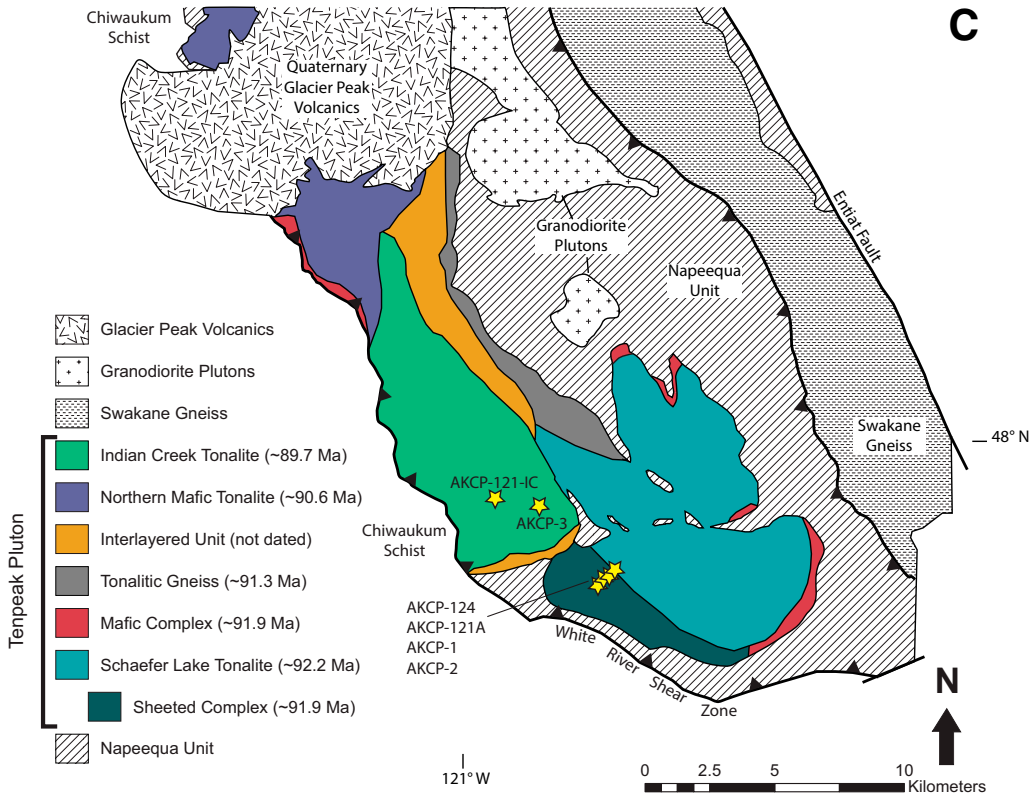

Figure 2. (*continued*). (C) Geologic map of the Tenpeak pluton (modified from Miller et al., 2009). Stars on A and B represent sample locations. Stars on C represent geochronologic sample locations (Shea, 2014; Chan et al., 2017).

and hornblendite that is interfingered with the Seven-Fingered Jack pluton (Dustin, 2015). Tonalites in the Kelly Mountain pluton are impossible to differentiate from those in the Seven-Fingered Jack pluton in the field; because of this, we grouped rocks from these plutons together as the "Seven-Fingered Jack pluton."

Geology of the Tenpeak Pluton

The ca. 92–89 Ma Tenpeak pluton (Cater, 1982; Miller and Paterson, 1999; Matzel et al., 2006; Chan et al., 2017; Miller et al., 2018) is an irregularly shaped, elongate body that also intrudes the Napeequa unit (Figs. 1 and 2C). The southern margin of the Tenpeak pluton intrudes the Chiwaukum Schist; however, this contact is in part obscured by the NE-dipping, reverse-slip White River shear zone (Fig. 2C; VanDiver, 1967; Magloughlin, 1986). Al-in-hornblende barometry (Brown and Walker, 1993; Dawes, 1993; Miller et al., 2009) and the presence of magmatic epidote (Zen, 1988) imply crystallization pressures around 0.7–1.0 GPa, suggesting an emplacement depth of ~20–35 km.

Geochemical and isotopic work by Dawes (1993), DeBari et al. (1998), Matzel et al. (2008), Chan et al. (2017), and Miller et al. (2018) suggests that rocks in the Tenpeak pluton were derived from mixing between mantle-derived mafic magma and crustally derived felsic magma (Miller et al., 2018). Noncumulate rocks of the Tenpeak pluton span a range of compositions from 51 to 66 wt% SiO_2 and 2–8 wt% MgO (Miller et al., 2018). Increasing La/Yb with SiO_2, relatively high Dy/Yb, and decreasing Y and Yb with increasing SiO_2 suggest the presence of garnet at some point during magma genesis and/or differentiation in nearly all samples (DeBari et al., 1998). Isotopically, the Tenpeak pluton shows a limited a range of whole-rock $\varepsilon_{Nd(t)}$ values ($\varepsilon_{Nd[t]}$ = 3.7–5.1; Matzel et al., 2008; Miller et al., 2018).

Previous workers have separated the Tenpeak into six units, most of which have been dated: the Schaefer Lake tonalite (ca. 92.2 Ma), the Mafic complex (ca. 91.9 Ma), the Tonalitic (Flaser) gneiss (ca. 91.3 Ma), the Northern mafic tonalite (ca. 90.6 Ma), the Interlayered zone (undated), and the Indian Creek tonalite (ca. 89.7 Ma; Miller and Paterson, 1999; Matzel et al., 2006; Shea, 2014; Chan et al., 2017; Miller et al., 2018). Overall, the Tenpeak pluton is dominated by tonalite, but the Mafic complex is a discontinuous heterogeneous zone of mingled and sheeted gabbro, tonalite, and hornblendite (Fig. 2C; Cater, 1982; Miller and Paterson, 1999; Matzel et al., 2006).

ANALYTICAL METHODS

Whole-rock samples collected as part of this study were analyzed for major and trace elements at the Washington State University GeoAnalytical laboratory using a ThermoARL Advant'XP sequential X-ray fluorescence spectrometer (XRF) and Agilent 7700 inductively coupled plasma–mass spectrometer (ICP-MS). A detailed description of the sample preparation and XRF analysis following a single low-dilution Li-tetraborate fused bead procedure was described by Johnson et al. (1999). The samples analyzed using ICP-MS followed procedures described by Lichte et al. (1987), Jarvis (1988), and Longerich et al. (1990). The precision for REE and other trace elements was 5% and 10%, respectively.

Oxygen isotopes in zircon were measured from a subset of samples from the Seven-Fingered Jack intrusive complex and Tenpeak pluton. Zircons selected for in situ oxygen (O) and hafnium (Hf) isotopic analysis were mounted in epoxy, polished to approximately half their thickness, and imaged using a cathodoluminescence (CL) detector on a scanning electron microscope. The imaging for the zircon crystals used for the O analyses was conducted at the University of California–Los Angeles

(UCLA), and the zircon crystals used for the Hf analyses were imaged at Memorial University of Newfoundland (MUN). These images were used to guide the selection of points for analysis in order to avoid inclusions or obviously inherited cores. High-spatial-resolution zircon $\delta^{18}O$ values were analyzed using the UCLA CAMECA ims 1270 high-resolution ion microprobe. All analyses were conducted during a single session; settings and conditions were similar to those described in the supplementary data in Schmitt (2006). Our data are reported relative to the R33 internal standard (5.55‰ ± 0.04‰; Valley, 2003).

Zircon Hf isotope ratios were measured at the MUN Micro-Analysis Facility. We followed the methods of Fisher et al. (2011), with the exception that N_2 was added to the Ar carrier gas for increased sensitivity. The analyses were done using a Thermo Finnigan Neptune multicollector (MC) ICP-MS interfaced to a Geolas Pro 193 nm Ar-F excimer laser, operating at 10 Hz, 5 J/cm^2, and with a 50-µm-diameter spot size. The analyses on the Cascades zircon crystals were interspersed with secondary reference zircon samples Plešovice, MUNZirc 2 and MUNZirc 4, and R-33, with measured ratios agreeing (within 1 standard deviation [SD]) with published solution (S)-MC-ICPMS isotopic compositions (see Fisher et al., 2011). The cup configuration, analytical methodology, and data reduction protocol were described in more detail by Fisher et al. (2011). Initial ε_{Hf} values were calculated using a chondritic uniform reservoir (CHUR) value of $^{176}Hf/^{177}Hf = 0.282785$, as reported by Bouvier et al. (2008).

RESULTS

Major- and Trace-Element Chemistry

Whole-rock major- and trace-element data are summarized here for: 14 samples from the Black Peak intrusive complex (11 new analyses and 3 analyses from Chan, 2012); 16 samples from the Seven-Fingered Jack pluton (2 new analyses, 6 analyses from Dustin, 2015, and 8 analyses from Elkins, 2015); and 75 samples of the Tenpeak pluton (19 analyses from Chan et al., 2017, and 56 analyses from Miller et al., 2018). The major- and trace-element results and the coordinates for sample locations are given in the GSA Data Repository Item (Table S1)[1].

Samples of igneous rocks from all three intrusions are classified as calc-alkaline (Fig. S1 [footnote 1]; Miyashiro, 1974) and fall within the diorite-tonalite-granodiorite-granite suite using the classification of Cox et al. (1979) (Fig. S2 [footnote 1]). They are metaluminous to slightly peraluminous with a range in Al_2O_3 (13–21 wt%, with one outlier at 8 wt%; Fig. S3 [footnote 1]; Shand, 1943). SiO_2 varies from 45.6 to 73.8 wt%, and all three intrusions show decreasing TiO_2, FeO, MgO, and CaO and increasing K_2O with increasing SiO_2 (Fig. 3). Al_2O_3 and P_2O_5 show considerable scatter below 55 wt% SiO_2 and a general decreasing trend above 55 wt% SiO_2.

Trace-element data from samples of the Black Peak intrusive complex, Seven-Fingered Jack pluton, and Tenpeak pluton have primitive mantle–normalized trace-element patterns characterized by light rare earth element (LREE) enrichment and HREE depletion (Fig. 4). Most samples lack a significant positive or negative Eu anomaly. Samples have an overall enrichment in large ion lithophile elements (LILEs), depletion of Nb and Ta relative to U and La, and pronounced positive Pb anomalies.

Black Peak Intrusive Complex

Although the majority of the Black Peak intrusive complex is composed of tonalite and granodiorite, the samples studied span a considerable range in composition, and SiO_2 varies accordingly between 51 and 72 wt%. MgO varies between 1 and 6 wt%. Black Peak samples have a more limited range of Al_2O_3 (15–17 wt%) than the other two plutons. Harker diagrams of the major oxides (e.g., MgO, CaO, FeO*) form a linear trend, although K_2O shows appreciable scatter (Fig. 3).

Trace elements from the Black Peak intrusive complex are characteristic of arc rocks and show enrichment in LILEs and depletion in high field strength elements (HFSEs; Fig. 4A). Black Peak samples display moderate to steep REE patterns ($[La/Yb]_N = 5.2–21.3$; Figs. 5A and 6A). Dy/Yb is high ($1.25 < [Dy/Yb]_N < 2$; Fig. 6B). $[La/Yb]_N$ and $[Dy/Yb]_N$ increase with SiO_2 (Figs. 6A and 6B). LREE/MREE is generally high ($1.2 < [La/Nd]_N < 2.5$) and broadly increases with SiO_2 (Fig. S4 [footnote 1]). MREE/HREE varies from moderate to high ($1.5 < [Gd/Yb]_N < 3.5$) and increases with SiO_2 (Fig. S5 [footnote 1]). Samples are characterized by small Eu anomalies that range from positive to negative (Fig. 5A). Sr/Y generally increases with SiO_2 and varies between ~20 and 180 (Fig. 6C).

Seven-Fingered Jack Pluton

Similar to Black Peak intrusive complex, most of the Seven-Fingered Jack pluton is tonalitic. However, a wide range of compositions was observed; SiO_2 varies from 50 to 70 wt%, and MgO varies from 1 to 6 wt%. Al_2O_3 ranges from 16 to 21 wt%, although the majority of analyses are between 16 and 18 wt%. Harker diagrams of the major oxides (e.g., MgO, CaO, FeO*) show a linear trend, but TiO_2, Na_2O, K_2O, and P_2O_5 show considerable scatter (Fig. 3).

Also, like the Black Peak intrusive complex, rocks from the Seven-Fingered Jack pluton are enriched in LILEs and depleted in HFSEs (Fig. 4B). REE patterns are moderate to steep ($[La/Yb]_N = 2.6–9.7$; Figs. 5B and 6A). Dy/Yb is moderate ($1.4 < [Dy/Yb]_N < 1.5$; Fig. 6B). Both $[La/Yb]_N$ and $[Dy/Yb]_N$ decrease with SiO_2 (Figs. 6A and 6B). LREE/MREE is generally moderate ($0.9 < [La/Nd]_N < 2$; Fig. S4 [footnote 1]) and has no clear relationship with SiO_2. MREE/HREE varies from moderate to high ($1.8 < [Gd/Yb]_N < 2.9$; Fig. S5 [footnote 1]) and has no clear relationship with SiO_2. Some samples have slightly negative Eu anomalies, while others have none (Fig. 5B). Unlike data from the Black Peak intrusive complex and the Tenpeak pluton, Sr/Y data from the Seven-Fingered Jack pluton show no clear relationship with SiO_2 and vary between ~20 and 40 (Fig. 6C).

Tenpeak Pluton

Samples from the Tenpeak pluton span a wide compositional range: from 50 to 73 wt% SiO_2 and 1–8 wt% MgO. Al_2O_3 ranges from 14 to 20 wt%. Harker diagrams show broadly linear trends for all the major oxides (e.g., MgO, CaO, FeO*), excepting Al_2O_3, which has considerable scatter (Fig. 3; Miller et al., 2018).

As summarized by Miller at al. (2018), trace elements in the Tenpeak pluton are enriched in LILEs and depleted in HFSEs (Fig. 4C). REE patterns are generally moderate to steep ($2.6 < [La/Yb]_N < 24.9$), with some very steep outliers ($[La/Yb]_N > 30$; Figs. 5C and 6A). Dy/Yb is moderate to high ($1.3 < [Dy/Yb]_N < 2.4$; Fig. 6). $[La/Yb]_N$ and $[Dy/Yb]_N$ increase with SiO_2 (Figs. 6A and 6B). LREE/MREE is moderate to high ($0.8 < [La/Nd]_N < 4.7$; Fig. S4 [footnote 1]) and generally increases with increasing SiO_2. MREE/HREE varies from moderate to very high ($1.5 < [Gd/Yb]_N < 5.2$; Fig. S5 [footnote 1]) and broadly increases with SiO_2. Eu anomalies are generally absent or slightly positive (Fig. 5C). Sr/Y generally increases with SiO_2 and varies between ~20 and 100 (Fig. 6C).

[1]GSA Data Repository Item 2018356, Supplementary text and figures, and data tables, is available at http://www.geosociety.org/datarepository/2018, or on request from editing@geosociety.org.

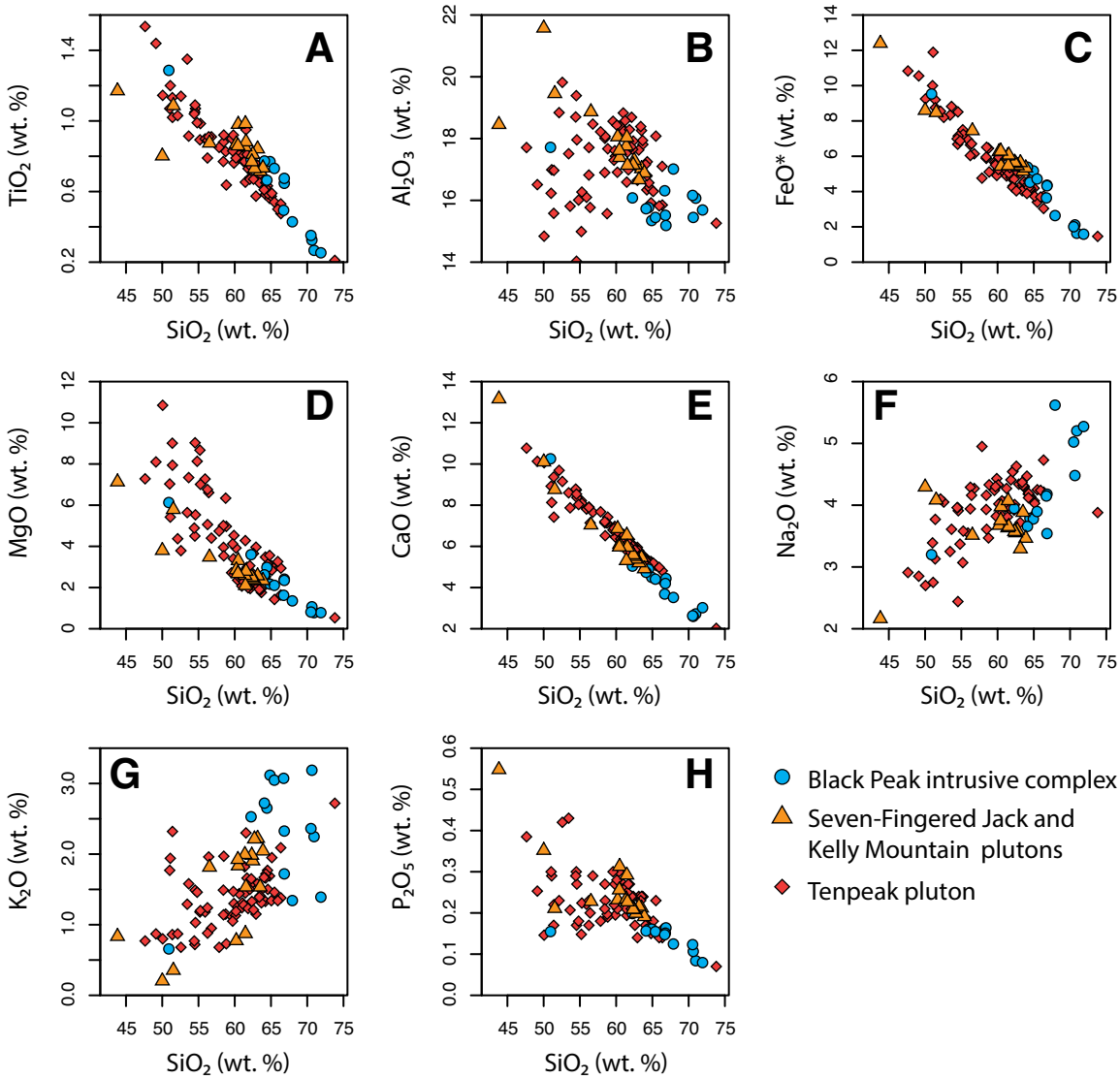

Figure 3. Variation diagrams of whole-rock major elements vs. SiO_2 content (in wt%): (A) TiO_2, (B) Al_2O_3, (C) FeO*, (D) MgO, (E) CaO, (F) Na_2O, (G) K_2O, and (H) P_2O_5. Symbols are described in the legend.

Oxygen and Hafnium Isotope Data

New in situ zircon oxygen isotopic data are presented here from six samples of the Tenpeak pluton and two samples of the Seven-Fingered Jack pluton, and these are compared to five published analyses from the Black Peak intrusive complex (Shea et al., 2016). New in situ zircon Hf isotopic data are presented from four samples of the Black Peak intrusive complex.

Zircon oxygen isotope data were obtained from representative samples of each of the three plutons (Fig. 7). Multiple (6–12) zircon crystals were analyzed for each sample, and some zircons were analyzed in more than one location. All data are presented in Figure 7 and the Data Repository (Table S1 [footnote 1]). Analyses of zircons from five samples from the Black Peak intrusive complex are summarized from Shea et al. (2016). Average zircon $\delta^{18}O$ values from Black Peak intrusive complex samples range from 6.5‰ (MAF) to 7.0‰ (PX10–86). Average zircon $\delta^{18}O$ values from the two samples of the Seven-Fingered Jack pluton are 6.4‰ and 7.7‰. Average zircon $\delta^{18}O$ values from six samples of the Tenpeak pluton range from 7.3‰ (PX10–243A) to 8.2‰ (IC2), although most samples have values between 7.5‰ and 8‰ (Fig. 7). Uncertainties (1 SD) for all data points are 0.55‰.

Zircon Hf isotopes were obtained from representative zircons from four samples of the Black Peak intrusive complex. Multiple (4–7) zircon crystals were analyzed for each sample, and some zircons were analyzed in more than one location (where it was clear in the CL images that there was no inherited core). All data are presented in Figure S6 and the Data Repository (Table S1 [footnote 1]). Average initial ε_{Hf} values from these samples range from ε_{Hf} = 9.26 (PX10–236) to ε_{Hf} = 8.11 (PX10–221), although individual spot analyses vary between ε_{Hf} = 10.10 and ε_{Hf} = 7.04 (Fig. S6 [footnote 1]). No Hf isotopic data were obtained from the Seven-Fingered Jack or Tenpeak plutons.

DISCUSSION

The Black Peak, Seven-Fingered Jack, and Tenpeak intrusions provide three views of contemporaneous magmatism in the same arc. Each

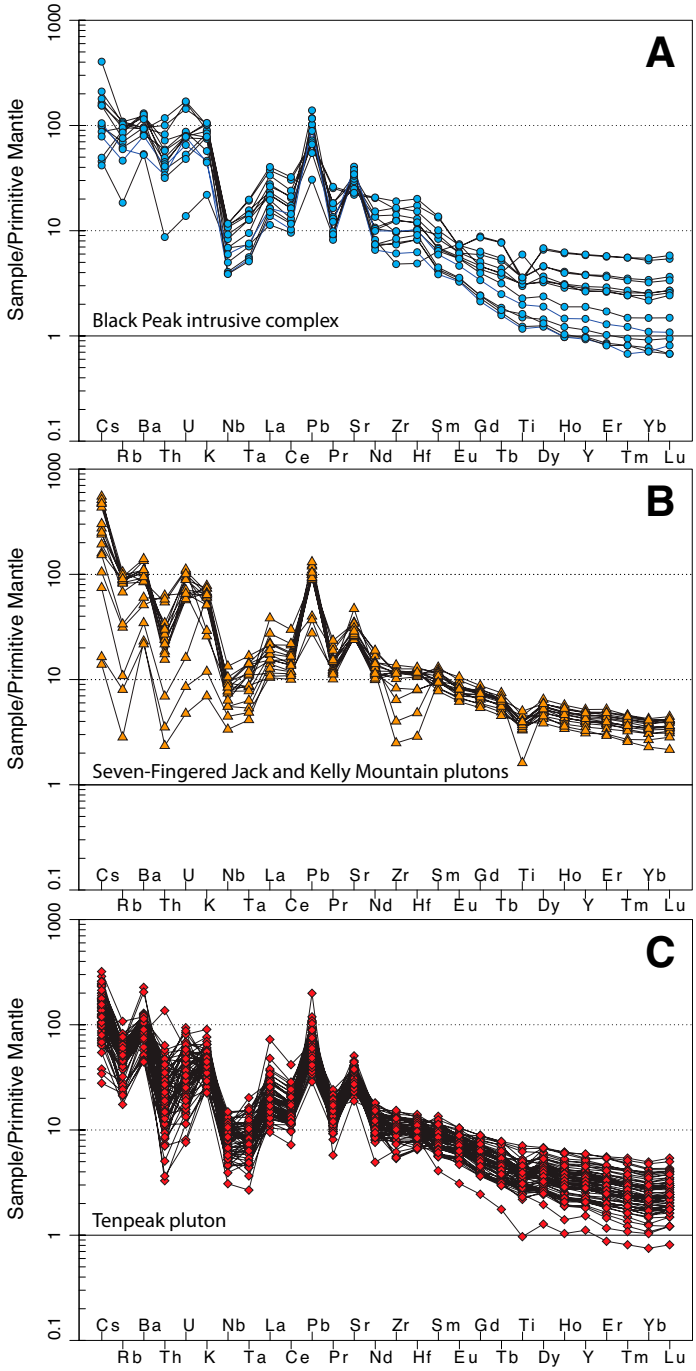

Figure 4. Primitive mantle–normalized (Sun and McDonough, 1989) multi-trace-element diagram of the studied samples. (A) Black Peak intrusive complex. (B) Seven-Fingered Jack pluton. (C) Tenpeak pluton.

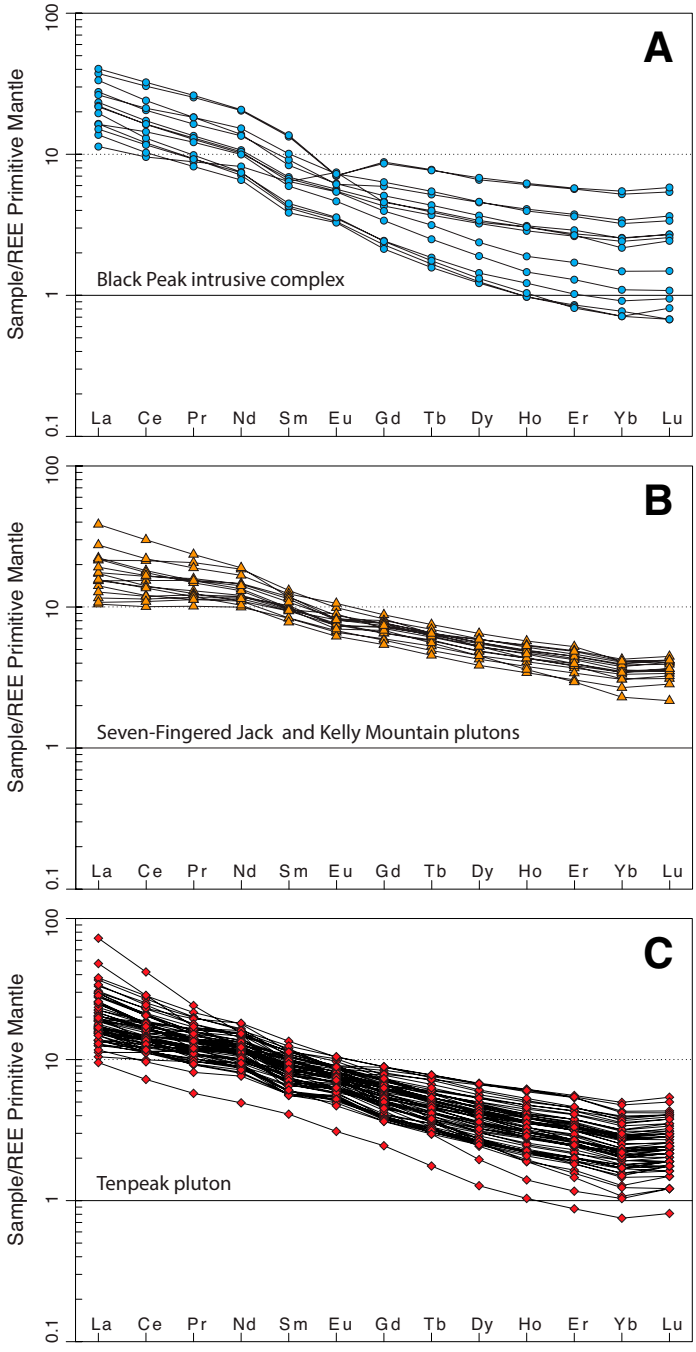

Figure 5. Primitive mantle–normalized (Sun and McDonough, 1989) rare earth element (REE) diagrams of the studied samples. (A) Black Peak intrusive complex. (B) Seven-Fingered Jack pluton. (C) Tenpeak pluton.

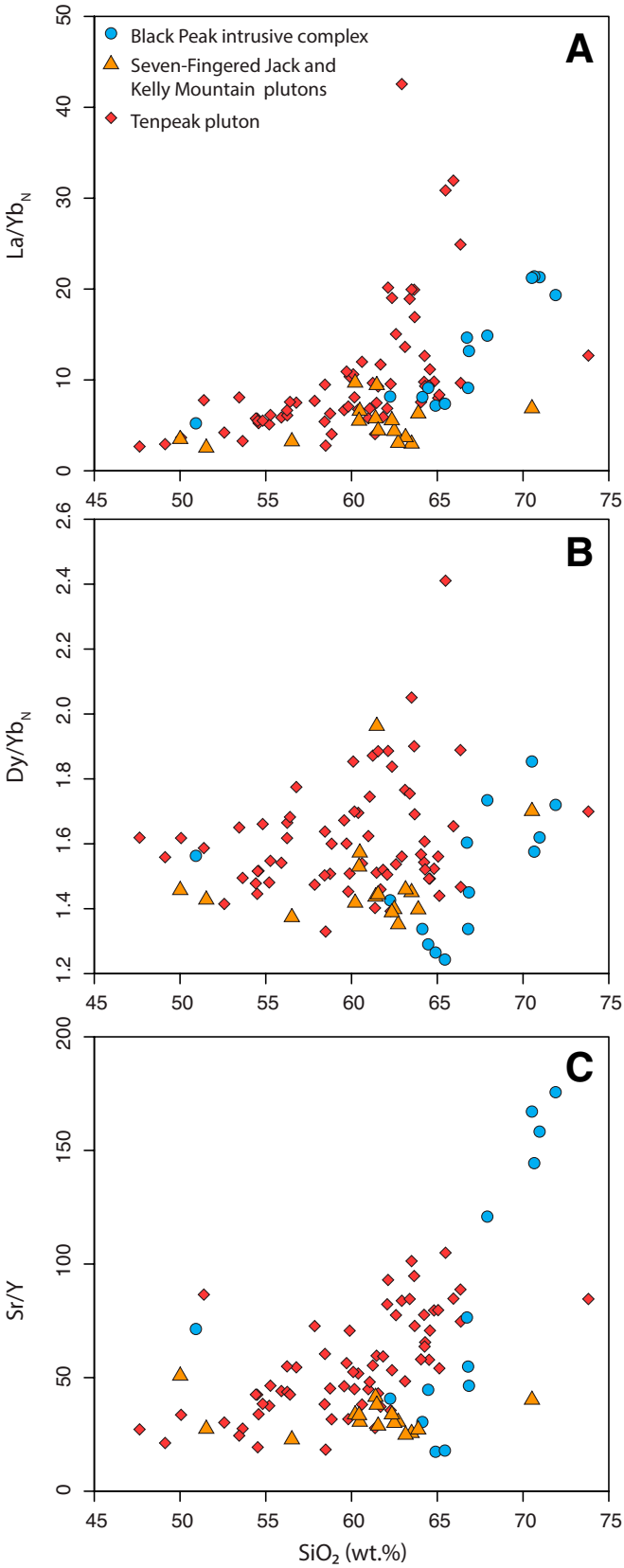

Figure 6. Primitive mantle–normalized (Sun and McDonough, 1989) ratios for samples from the Black Peak intrusive complex (circles), the Seven-Fingered Jack pluton (triangles), and the Tenpeak pluton (diamonds): (A) La/Yb (La/Yb$_N$) vs. SiO$_2$; (B) Dy/Yb (Dy/Yb$_N$) vs. SiO$_2$; and (C) Sr/Y vs. SiO$_2$.

intrusion was emplaced at a different crustal level, ranging from relatively shallow (Black Peak intrusive complex), to intermediate (Seven-Fingered Jack pluton), to deep (Tenpeak pluton). Major elements in these plutons show a broad trend toward more-evolved compositions (e.g., higher silica, lower FeO*, lower MgO) in progressively shallower plutons (Fig. 3). All three plutons generally become more felsic and homogeneous with time (Fig. 8). Because these plutons are not linked spatially (they are separated by ~60 km across strike; Fig. 1), it is impossible to know whether they were connected at depth to a broader melt source region. However, their major-element geochemistry is suggestive of a connected melt source region for all three plutons (Fig. 3).

REE Patterns in North Cascades Plutons

The most-striking feature in our geochemical data set is a significant depletion in HREE in samples from the Black Peak intrusive complex and the Tenpeak pluton (Figs. 5A and 5C). Samples from the Seven-Fingered Jack pluton show a moderate HREE depletion that is less pronounced than in the other intrusions (Fig. 5B). HREE depletion is commonly associated with the presence of amphibole and/or garnet in the lower crust (e.g., Mamani et al., 2010; Profeta et al., 2015). Amphibole and/or garnet in the deep crust may form as a restite caused by partial melting in the deep crust (e.g., Hildreth and Moorbath, 1988; Hanchar et al., 1994) or as a cumulate from fractional crystallization (e.g., Müntener et al., 2001; Alonso-Perez and Müntener, 2009). In either case, the lower crust of the arc must reach high-pressure conditions in order for garnet to stabilize (~1.2 GPa; Alonso-Perez and Müntener, 2009). It is possible to determine the presence of garnet in the melt region by using trace-element geochemistry: Magmatic equilibration with garnet during partial melting or fractional crystallization generally increases both La/Yb and Dy/Yb versus SiO$_2$, while equilibration with amphibole generally increases La/Yb versus SiO$_2$ and decreases Dy/Yb versus SiO$_2$ (Macpherson et al., 2006; Davidson et al., 2007). Note also, that for Black Peak and most Tenpeak samples, the lack of an Eu anomaly is also consistent with no appreciable role for plagioclase in either fractionation or melting.

Both the Black Peak intrusive complex and the Tenpeak pluton show a positive correlation between La/Yb$_N$ and SiO$_2$, but the Seven-Fingered Jack pluton has considerable scatter (Fig. 6A). The Black Peak intrusive complex shows a positive correlation between Dy/Yb$_N$ and SiO$_2$ for the entire data set; however, close inspection suggests a negative correlation between Dy/Yb$_N$ and SiO$_2$ until ~66 wt% SiO$_2$, at which point the correlation becomes distinctly positive (Fig. 6B). The Tenpeak pluton has a more scattered but overall positive correlation between Dy/Yb$_N$ and SiO$_2$ (Fig. 6B). No obvious correlation between Dy/Yb$_N$ and SiO$_2$ is observed for the Seven-Fingered Jack pluton (Fig. 6B).

The La/Yb$_N$ and Dy/Yb$_N$ versus SiO$_2$ data from the Black Peak intrusive complex suggest that samples with <66 wt% SiO$_2$ may have solidified from magmas that equilibrated with amphibole (although this conclusion is based on a limited data set), and that more-evolved samples (>66 wt% SiO$_2$) likely solidified from magmas that equilibrated with garnet (Fig. 6A). La/Yb$_N$ and Dy/Yb$_N$ versus SiO$_2$ data from the Tenpeak pluton are less definitive, but they also indicate that magmas equilibrated with garnet during fractionation and/or partial melting (Miller et al., 2018). In contrast, REE data from the Seven-Fingered Jack pluton suggest equilibration of magmas with hornblende.

High-precision CA-ID-TIMS geochronology on the same samples of the Black Peak intrusive complex that were used for whole-rock analyses allows us to also track these geochemical shifts temporally, indicating that the garnet signature in the complex appeared after 90 Ma (Fig. 9). Although we do not have geochronologic data for the entire Tenpeak

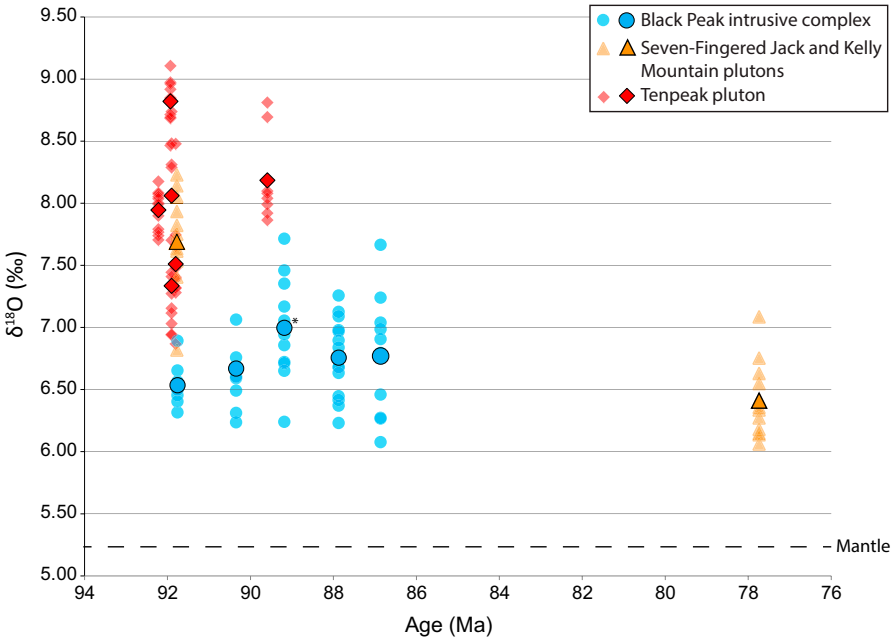

Figure 7. High-precision chemical abrasion–isotope dilution–thermal ionization mass spectrometry (CA-ID-TIMS) U-Pb zircon age (Ma) vs. zircon $\delta^{18}O$ for samples from the Black Peak intrusive complex (circles), the Seven-Fingered Jack pluton (triangles), and the Tenpeak pluton (diamonds). Each suite of symbols represents a distinct sample. Lighter symbols represent $\delta^{18}O$ for a single spot on a zircon; darker symbols with a black border represent the average $\delta^{18}O$ for each sample. 1σ errors for individual spot analyses are <0.1‰. Dashed line indicates mantle value (5.3‰; Valley, 2003). Asterisk indicates sample where one outlier at 10‰ was not included in the average $\delta^{18}O$ calculation. Zircon geochronology is from Shea (2014), Shea et al. (2016), and Chan et al. (2017). Typical uncertainty of sample ages is less than 100 k.y.

pluton sample suite, high-precision CA-ID-TIMS geochronology on a modest number of samples suggests that this signature evolved similarly (Fig. 9), and thus we infer that at the arc scale, the garnet signature becomes more pronounced after 90 Ma.

Isotopic Evidence for Crustal Melt

Zircon Hf isotopic data provide additional insight into the nature of crustal thickening in the North Cascades; because the mantle is isotopically different from crustal rocks, these data allow an investigation into magma source material (crustal vs. mantle input). The $\delta^{18}O$ values for zircons from the Tenpeak pluton show no obvious trend between ca. 92 Ma to ca. 89 Ma (Fig. 7). One sample from the Seven-Fingered Jack pluton was analyzed for $\delta^{18}O$ in zircon and has a value similar to that found in the Tenpeak pluton (Fig. 7). The $\delta^{18}O$ values for zircons from the Black Peak intrusive complex all overlap each other within uncertainty, although post–90 Ma zircons show a slight shift to higher average $\delta^{18}O$. Hafnium isotopic analyses on zircons from the Black Peak intrusive complex all overlap within uncertainty but show a 1 ε_{Hf} unit negative shift in the average ε_{Hf} (from an average of approximately +9.2 to an average of +8.2) after 90 Ma (Fig. S6 [footnote 1]). These values require a source that was relatively immature, but they are less than expected for pristine Late Cretaceous depleted mantle (+12 to +16; Vervoort and Blichert-Toft, 1999). There is a fairly striking contrast in zircon $\delta^{18}O$ values between the Tenpeak and the Black Peak intrusions, with the Tenpeak rocks being isotopically heavier in O isotopic composition. Zircon $\delta^{18}O$ in all samples and zircon ε_{Hf} from the Black Peak intrusive complex indicate that magmas in the three intrusions are not "pure" mantle-derived melts. Using simple binary mixing models based on oxygen isotopes, it is possible to estimate the relative contributions from crustal and mantle components, assuming $\delta^{18}O$ in zircon approximates the $\delta^{18}O$ value in the magma from which it crystallized. Using a value of 15‰, which is near the upper range of values for the Chiwaukum Schist (host rock to the southwestern Tenpeak pluton; Anderson et al., 2012) and similar to typical altered oceanic crust values (Lackey et al., 2005), and a canonical mantle $\delta^{18}O$ of 5.3‰ (Valley, 2003), we estimate between 20% (PX10–243A) and 30% (TP30) crustal component in the Tenpeak pluton and between 10% (MAF-1) and 20% (PX10–86) in the Black Peak intrusive complex (Shea et al., 2016). We note, however, that these are conservative estimates, because the assimilant could be isotopically lighter, and the host rocks of these intrusions are generally immature accreted oceanic and arc rocks.

The contrast in zircon $\delta^{18}O$ values between the Black Peak and Tenpeak intrusions indicates either that melt sources for the Black Peak intrusive complex and Tenpeak pluton were isotopically different, or that isotopically similar primary arc magmas assimilated isotopically distinct contaminants. The principal exposed host rocks into which both plutonic complexes were intruded are compositionally similar (Fig. 1; Chiwaukum Schist/Napeequa unit and the correlative Twisp Valley schist), suggesting the latter explanation is less likely. Although part of the Black Peak intrusive complex intruded into greenschist-facies metamorphosed sediments of the Methow basin along its eastern margin, there is limited field evidence for assimilation of these host rocks into the intruding pluton at the level of emplacement. It is unlikely that the small volume of sediments assimilated along this contact significantly contributed to the isotopic signature of the entire complex. The isotopic differences may reflect (1) isotopic domains in the melt sources that varied within the arc depending on the composition and lithology of the deep crust, or (2) more effective assimilation and partial melting of host rock in the deep crust (Tenpeak pluton) than at shallow levels (Black Peak intrusive complex).

Although there is a slight shift in zircon Hf and O isotopic values with time in the Black Peak samples as noted above, the data set as a whole for both the Tenpeak and Black Peak rocks suggests that the contribution from crustal sources shifted little over the lifetime of both plutons. Perhaps most important for this study is that the zircon isotopic data show that magmatic differentiation involved the crust throughout the lifetime of these intrusions. No zircons analyzed had $\delta^{18}O$ and ε_{Hf} values indicative of pristine mantle ($\delta^{18}O \approx 5.3‰$; Valley et al., 2003; $\varepsilon_{Hf} \approx +12–16$; Vervoort and Blichert-Toft, 1999), and thus the shift in trace-element patterns with time must reflect changes resulting from processes in the deep crust—remelting of arc crust or deep-crustal assimilation accompanying fractional crystallization.

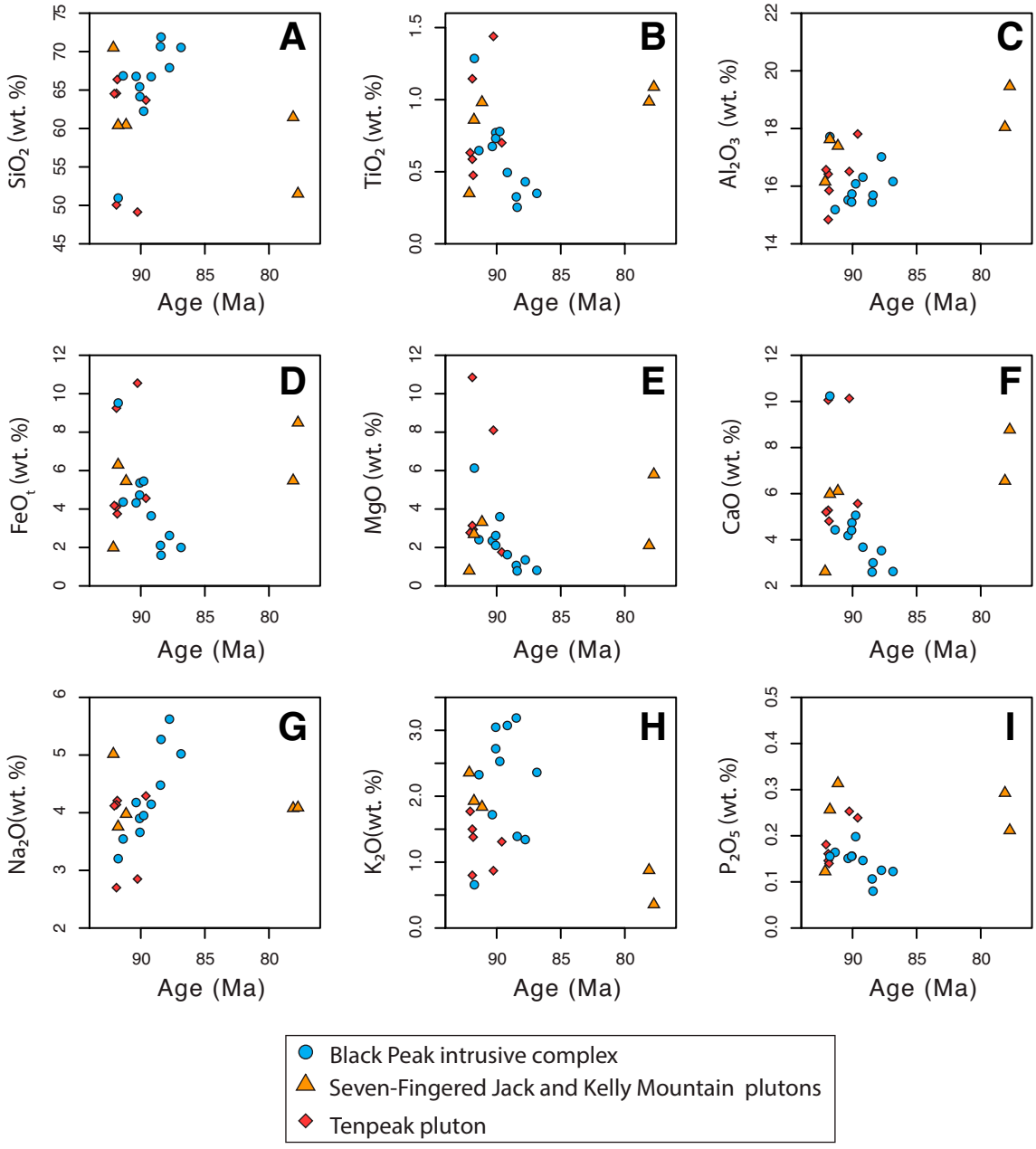

Figure 8. Variation diagrams of high-precision chemical abrasion–isotope dilution–thermal ionization mass spectrometry (CA-ID-TIMS) U-Pb zircon age (Ma) vs. whole-rock major elements: (A) SiO_2, (B) TiO_2, (C) Al_2O_3, (D) FeO*, (E) MgO, (F) CaO, (G) Na_2O, (H) K_2O, and (I) P_2O_5. Samples from the Black Peak intrusive complex and Seven-Fingered Jack pluton were individually dated. Samples from the Tenpeak pluton are grouped based on the age of the unit from which they were collected. Symbols are described in legend. Zircon geochronology is from Shea (2014), Shea et al. (2016), and Chan et al. (2017). Typical uncertainty of sample ages is less than 100 k.y.

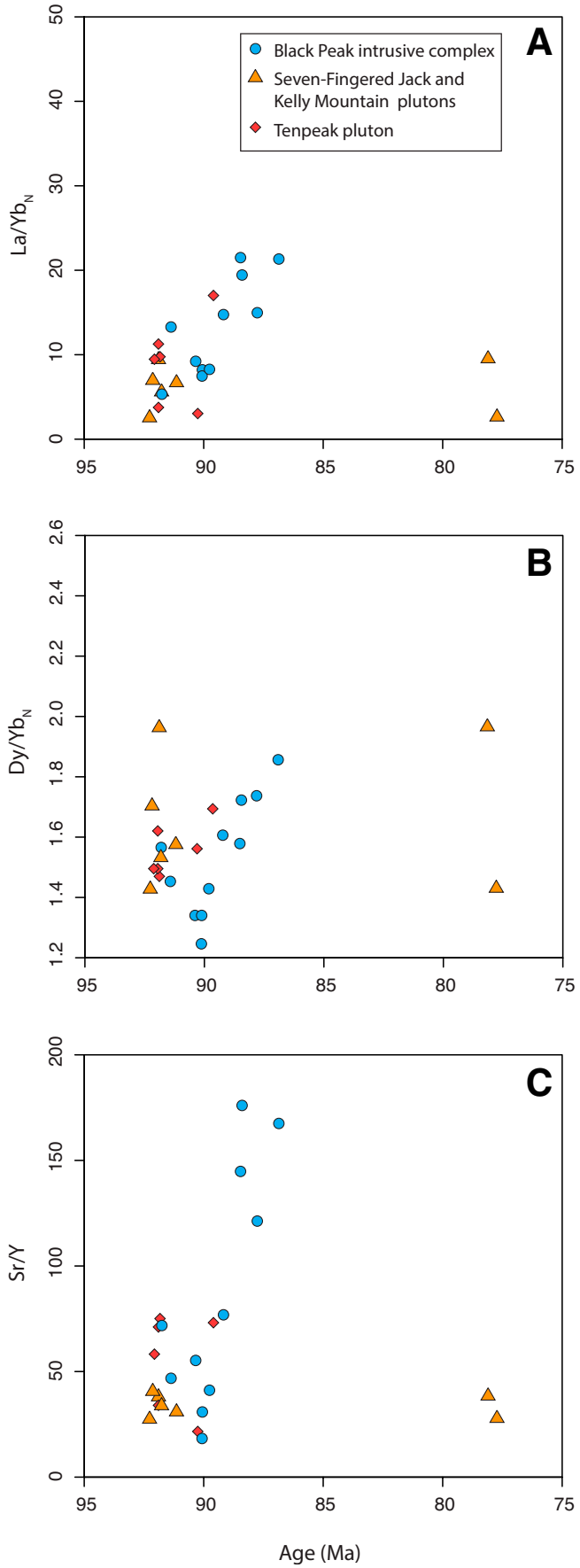

Figure 9. Primitive mantle–normalized (Sun and McDonough, 1989) ratios for dated samples from the Black Peak intrusive complex (circles), the Seven-Fingered Jack pluton (triangles), and the Tenpeak pluton (diamonds). (A) La/Yb (La/Yb$_N$) vs. high-precision chemical abrasion–isotope dilution–thermal ionization mass spectrometry (CA-ID-TIMS) U-Pb zircon age (Ma). (B) Dy/Yb (Dy/Yb$_N$) vs. high-precision CA-ID-TIMS U-Pb zircon age (Ma). (C) Sr/Y vs. high-precision CA-ID-TIMS U-Pb zircon age (Ma). Zircon geochronology is from Shea (2014), Shea et al. (2016), and Chan et al. (2017). Typical uncertainty of sample ages is less than 100 k.y.

Evidence for Late, Thick Crust in the North Cascades Arc

Several recent studies have correlated crustal thickness in magmatic arcs with trace-element ratios; in particular, increasing Sr/Y in arc rocks has been linked to an increase in crustal thickness in the North American Cordillera during the Mesozoic (Schwartz et al., 2014; Chapman et al., 2015; Profeta et al., 2015), in Mesozoic Fiordland intrusions (Schwartz et al., 2017), in the Central Andes during the Cenozoic (Profeta et al., 2015), and in a global data set of Pliocene–Quaternary arcs (Chiaradia, 2015).

Sr/Y values in our data set are positively correlated with SiO_2 (Fig. 6C) and with time (Fig. 9C) but are negatively correlated with Y (Fig. S7 [footnote 1]). We interpret these correlations and the shift in REE patterns (Fig. 5) and key REE ratios (La/Yb$_N$, and Dy/Yb$_N$; Figs. 6B and 6C) as evidence that the arc matured and thickened during the time interval over which these intrusions were emplaced, and that the deep crust eventually reached pressures that stabilized garnet (Müntener et al., 2001; Alonso-Perez and Müntener, 2009).

Crustal thickening can be caused by underthrusting of the retroarc lithosphere (e.g., DeCelles et al., 2009), imbrication and shortening of the forearc (e.g., Sauer et al., 2017), intra-arc crustal shortening and magmatic thickening (e.g., Jagoutz and Schmidt, 2013; Cao et al., 2016), and/or relamination (e.g., Hacker et al., 2011). Although a combination of these processes may have operated in the North Cascades, evidence suggests that crustal thickening was dominated by regional NE-SW horizontal shortening (e.g., Misch, 1966; Brandon et al., 1988; Miller et al., 2009). This evidence includes thermobarometry of host rocks for a number of 96–90 Ma plutons that indicate pressure increases of up to 0.5 GPa (Brown and Walker, 1993; Miller et al., 1993; Whitney et al., 1999) along with contact aureoles showing evidence for andalusite overprinted by kyanite. Geothermobarometry also indicates that supracrustal rocks were buried to depths of 25–40 km in many parts of the arc (Whitney et al., 1999; Valley et al., 2003).

Regional-scale shortening in the North Cascades has been linked to the collision of the Insular superterrane with the Intermontane superterrane (Rubin et al., 1990) between ca. 100 Ma and 90 Ma, contemporaneous with the mid-Cretaceous magmatic flare-up in the region between 96 and 89 Ma (Miller et al., 2009). This shortening was expressed at shallow levels by SW-directed thrusting and at deep levels by ductile folding, cleavage development, SW-directed reverse shear, and subhorizontal orogen-parallel stretching (Miller et al., 2006). Recent U-Pb and Hf isotope work on detrital zircons from the metasedimentary host rocks of the Tenpeak, Seven-Fingered Jack, and Black Peak intrusions (Sauer et al., 2017) suggested that thickening involved imbrication and deep thrusting of these sequences in the arc at approximately the same time as emplacement of the intrusions. The development of a depleted HREE signature and the pronounced shift in Sr/Y and La/Yb$_N$ ratios in the Black Peak intrusive complex and the Tenpeak pluton can be interpreted as evidence for the stabilization of garnet in the lower crust of the arc beginning around 90 Ma, near the end of both the magmatic flare-up and a major period of shortening in the North Cascades (Fig. 10). Post–89 Ma intrusions in the

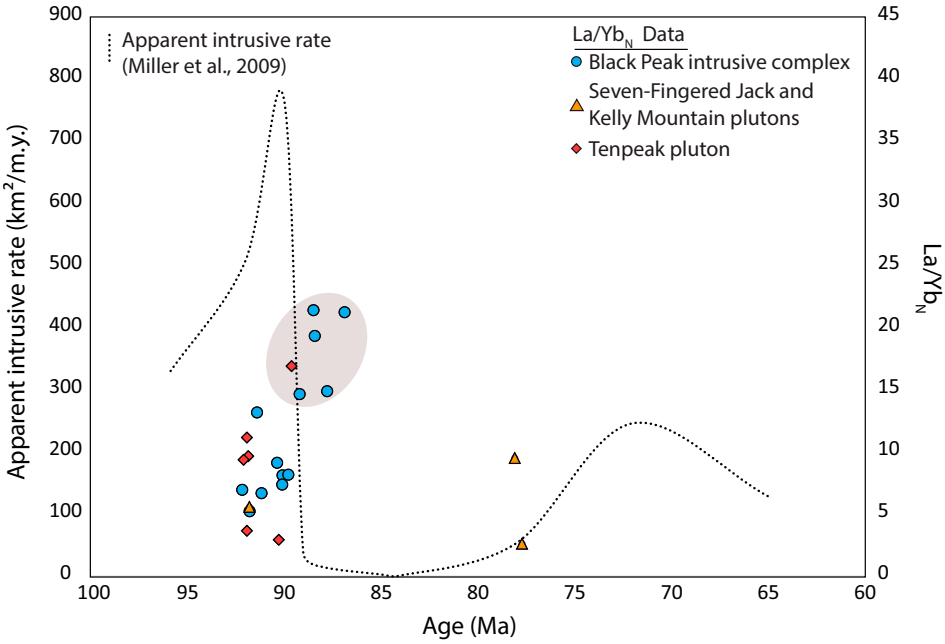

Figure 10. Apparent intrusive rate (in km²/m.y.) vs. age (Ma) for the North Cascades with La/Yb$_N$ vs. age data overlain. The left vertical axis shows variations in apparent intrusive rate (shown as dashed line) from Miller et al. (2009). The right vertical axis is scaled for La/Yb$_N$. Note how the La/Yb$_N$ data generally show higher values after 90 Ma (shaded region), approximately the same time as the end of the magmatic flare-up.

Black Peak intrusive complex have progressively more depleted HREE signatures, suggesting further development of garnet in the lower crust, even as magmatic activity waned (Fig. 10).

Garnet in the lower crust may be the product of fractional crystallization of mantle-derived melts where garnet is stable (e.g., Müntener et al., 2001; Alonso-Perez and Müntener, 2009) or may be due to the burial and subsequent partial melting of preexisting (possibly cogenetic) lower-crustal rocks in the garnet stability field. These data support a model wherein a major episode of horizontal crustal shortening (between ca. 100 Ma and 90 Ma) and a contemporaneous magmatic flare-up (96–89 Ma) caused crustal thickening that shifted the melt source to pressures high enough to stabilize garnet. The lack of pronounced variation in zircon $\delta^{18}O$ and ε_{Hf} with time suggests that the isotopic composition of magma did not change significantly while the crust was thickening. In each pluton, magma produced during the flare-up (pre–90 Ma) is not appreciably different isotopically from magma produced after the end of the flare-up (post–90 Ma), although the distinctly different zircon $\delta^{18}O$ values between the Black Peak and Tenpeak samples may reflect isotopic provinciality in melt source regions of the two intrusions. The absence of any marked change in $\delta^{18}O$ and ε_{Hf} suggests that intra-arc shortening and magmatic addition may have been responsible for crustal thickening (e.g., Jagoutz and Schmidt, 2013; Cao et al., 2016; Sauer et al., 2017). This thickening caused the magma source region to migrate to depths below the stability threshold for garnet, resulting in the production of melts with depleted HREE signatures. The appearance of the garnet signature shortly (<1 m.y.) before the cessation of the mid-Cretaceous flare-up in the North Cascades requires that shortening was concurrent with the flare-up, reaching maximum crustal thickness (i.e., garnet stability) toward the terminal stages of the flare-up (Fig. 10). Karlstrom et al. (2014) and Chin et al. (2015) elucidated how thickening may result in the cessation of arc flare-up magmatism, rather than serving as a trigger (e.g., DeCelles et al., 2009), and it is intriguing to postulate, given the timing constraints presented here, that thickening into the garnet stability field may have ultimately led to the cessation of the Cretaceous flare-up in the North Cascades around 89 Ma.

Based on work in the Early Cretaceous Chelan Complex of the North Cascades, Dessimoz et al. (2012) suggested that hornblende fractionation played an important role in the production of peraluminous, high-Sr/Y tonalitic melts in the arc. However, existing U-Pb geochronologic data suggest that the Chelan Complex represents an earlier period of magmatism (possibly much earlier) that preceded the peak magmatic flare up (96–89 Ma) in the North Cascades (Mattinson, 1972; Hopson and Mattinson, 1994; Mattinson et al., 2014; Miller et al., 2009). In general, our data are not inconsistent with an earlier role for hornblende fractionation, but we maintain that our geochronologic and geochemical data clearly document a role for garnet fractionation that was coincident with intra-arc shortening and the flare-up in the North Cascades.

Data from younger (post–flare-up) intrusions in the North Cascades, including a small data set from the 72 Ma Cardinal Peak pluton (Parent, 1999), suggest that this garnet signature (and by implication, thicker crust) may have persisted for over 15 m.y. Late Cretaceous (100–80 Ma) rocks of the Coast plutonic complex in central British Columbia also show a similar garnet signature (Girardi et al., 2012) that is broadly synchronous with the major flare-up of magmatism there, suggesting that thickening affected a large area of the arc.

CONCLUSIONS

Data from several Cretaceous plutons support the origin of the North Cascades in a continental magmatic arc built on juvenile arc lithosphere and show a general trend toward more-evolved magmas with time and with decreasing depth. Elevated La/Yb$_N$, Dy/Yb$_N$, and Sr/Y ratios in intrusions younger than 90 Ma indicate the presence of garnet in the lower crust following ~10 m.y. of regional shortening, crustal thickening, and magmatism associated with the collision of the Insular and Intermontane superterranes. The lack of evidence for any significant change in $\delta^{18}O$ values in the Black Peak intrusive complex or the Tenpeak pluton indicates that this was not caused by melting of deeply buried crustal material, but instead it was related to crustal thickening, which was likely due to regional shortening and magmatism. This thickening may have contributed

to the waning and eventual cessation of the Cretaceous flare-up in the North Cascades around 89 Ma.

ACKNOWLEDGMENTS

Samuel Bowring's impact on this paper is unseen but felt in many ways. We are grateful for his long-standing enthusiasm for and support of research in the North Cascades. Careful and thoughtful reviews by Jay Chapman and an anonymous reviewer significantly improved the manuscript. This paper benefited from conversations with Seth Burgess, Frederick Frey, Tim Grove, Oli Jagoutz, and Erin Todd. Analytical assistance from Jahan Ramezani, Nilanjan Chatterjee, Frank Dudás, Rita Economos, Axel Schmitt, and Rebecca Lam is gratefully acknowledged. We are grateful to the Methow Valley Ranger District, Entiat Ranger District, and the North Cascades National Park for access. This research was supported by National Science Foundation grants EAR-0948388 to S. Bowring, EAR-0948685 to J. Miller and R. Miller, and EAR-1119358 to R. Miller.

REFERENCES CITED

Adams, J., 1964, Origin of the Black Peak quartz diorite, Northern Cascades, Washington: American Journal of Science, v. 262, p. 290–306, https://doi.org/10.2475/ajs.262.3.290.

Alonso-Perez, R., and Müntener, O., 2009, Igneous garnet and amphibole fractionation in the roots of island arcs: Experimental constraints on andesitic liquids: Contributions to Mineralogy and Petrology, v. 157, p. 541–558, https://doi.org/10.1007/s00410-008-0351-8.

Anderson, J.L., Morrison, J., and Paterson, S.R., 2012, Post-emplacement fluids and pluton thermobarometry: Mount Stuart batholith, Washington Cascades: International Geology Review, v. 54, p. 491–508, https://doi.org/10.1080/00206814.2012.663165.

Bouvier, A., Vervoort, J.D., and Patchett, P.J., 2008, The Lu-Hf and Sm-Nd isotopic composition of CHUR: Constraints from unequilibrated chondrites and implications for the bulk composition of terrestrial planets: Earth and Planetary Science Letters, v. 273, p. 48–57, https://doi.org/10.1016/j.epsl.2008.06.010.

Brandon, M.T., Cowan, D.S., and Vance, J.A., 1988, The Late Cretaceous San Juan Thrust System, San Juan Islands, Washington: Geological Society of America Special Paper 221, 81 p., https://doi.org/10.1130/SPE221-p1.

Brown, E.H., and Walker, N.W., 1993, A magma-loading model for Barrovian metamorphism in the southeast Coast plutonic complex, British Columbia and Washington: Geological Society of America Bulletin, v. 105, p. 479–500, https://doi.org/10.1130/0016-7606(1993)105<0479:AMLMFB>2.3.CO;2.

Cao, W., Kaus, B.J.P., and Paterson, S., 2016, Intrusion of granitic magma into the continental crust facilitated by magma pulsing and dike-diapir interactions: Numerical simulations: Tectonics, v. 35, p. 1575–1594, https://doi.org/10.1002/2015TC004076.

Cater, F.W., 1982, Intrusive Rocks of the Holden and Lucerne Quadrangles, Washington—The Relation of Depth Zones, Composition, Textures, and Emplacement of Plutons: U.S. Geological Survey Professional Paper 1220, 114 p.

Cater, F.W., and Crowder, D.F., 1967, Geologic Map of the Holden Quadrangle, Snohomish and Chelan Counties, Washington: U.S. Geological Survey Geologic Quadrangle Map GQ-646, scale 1:62,500.

Cater, F.W., and Wright, T.L., 1967, Geologic Map of the Lucerne Quadrangle, Chelan County, Washington: U.S. Geological Survey Geologic Quadrangle Map GQ-647, scale 1:62,500.

Chan, C.F., 2012, Constructing a sheeted magmatic complex within the lower arc crust: Insights from the Tenpeak pluton, North Cascades, Washington [M.S. Thesis]: Corvallis, Oregon State University, 333 p.

Chan, C., Shea, E., Kent, A., Miller, R., Miller, J., and Bowring, S., 2017, Formation of a sheeted magma complex within the lower crustal Tenpeak pluton, North Cascades, Washington: Geosphere, v. 13, p. 1610–1639, https://doi.org/10.1130/GES01323.1.

Chapman, J.B., Ducea, M.N., DeCelles, P.G., and Profeta, L., 2015, Tracking changes in crustal thickness during orogenic evolution with Sr/Y: An example from the North American Cordillera: Geology, v. 43, p. 919–922, https://doi.org/10.1130/G36996.1.

Chiaradia, M., 2015, Crustal thickness control on Sr/Y signatures of recent arc magmas: An Earth scale perspective: Scientific Reports, v. 5, p. 8115, https://doi.org/10.1038/srep08115.

Chin, E.J., Lee, C.-T.A., and Blichert-Toft, J., 2015, Growth of upper plate lithosphere controls tempo of arc magmatism: Constraints from Al-diffusion kinetics and coupled Lu-Hf and Sm-Nd chronology: Geochemical Perspective Letters, v. 1, p. 20–32, https://doi.org/10.7185/geochemlet.1503.

Cox, K.G., Bell, J.D., and Pankhurst, R.J., 1979, The Interpretation of Igneous Rocks: London, Allen and Unwin, 450 p., https://doi.org/10.1007/978-94-017-3373-1.

Davidson, J., Turner, S., Handley, H., Macpherson, C., and Dosseto, A., 2007, Amphibole "sponge" in arc crust?: Geology, v. 35, p. 787–790, https://doi.org/10.1130/G23637A.1.

Dawes, R., 1993, Mid-Crustal, Late Cretaceous Plutons of the North Cascades: Petrogenesis and Implications for the Growth of the Continental Crust [Ph.D. thesis]: Seattle, Washington, University of Washington, 272 p.

DeBari, S.M., Miller, R.B., and Paterson, S.R., 1998, Genesis of tonalitic plutons in the Cretaceous magmatic arc of the North Cascades; mixing of mantle-derived mafic magmas and melts of a garnet-bearing lower crust: Geological Society of America Abstracts with Programs, v. 30, no. 7, p. 257–258.

DeCelles, P.G., Ducea, M.N., Kapp, P., and Zandt, G., 2009, Cyclicity in Cordilleran orogenic systems: Nature Geoscience, v. 2, p. 251–257, https://doi.org/10.1038/ngeo469.

Dessimoz, M., Müntener, O., and Ulmer, P., 2012, A case for hornblende-dominated fractionation of arc magmas: The Chelan Complex (Washington Cascades): Contributions to Mineralogy and Petrology, v. 163, p. 567–589, https://doi.org/10.1007/s00410-011-0685-5.

Dragovich, J., Norman, D., Haugerud, R., and Miller, R., 1997, Geologic Map of the Gilbert 7.5′ Quadrangle, Chelan and Okanogan Counties, Washington: Washington Division of Geology and Earth Resources Geologic Map GM-46, 1 sheet, scale 1:24,000, 67 p.

Ducea, M., 2001, The California arc: Thick granitic batholiths, eclogitic residues, lithospheric-scale thrusting, and magmatic flare-ups: GSA Today, v. 11, no. 11, p. 4–10, https://doi.org/10.1130/1052-5173(2001)011<0004:TCATGB>2.0.CO;2.

Dustin, K., 2015, Structure, Construction, and Geochemistry of the Cretaceous Seven-Fingered-Jack Intrusive Complex in the Klone Peak Area, North Cascades, Washington [M.S. thesis]: San Jose, California, San Jose State University, 107 p.

Eddy, M.P., Bowring, S.A., Miller, R.B., and Tepper, J.H., 2016, Rapid assembly and crystallization of a fossil large-volume silicic magma chamber: Geology, v. 44, p. 331–334, https://doi.org/10.1130/G37631.1.

Elkins, S.W., 2015, Structure, construction, and geochemistry of the highly elongate Seven-Fingered-Jack pluton in the Devil's Smokestack area, North Cascades, Washington [M.S. thesis]: San Jose, California, San Jose State University, 101 p.

Fisher, C.M., Hanchar, J.M., Dhuime, B., Samson, S.D., Blichert-Toft, J., Vervoort, J.D., and Lam, R., 2011, Synthetic zircon doped with hafnium and rare earth elements for use as reference material for hafnium isotopic analyses: Chemical Geology, v. 286, p. 32–47, https://doi.org/10.1016/j.chemgeo.2011.04.013.

Girardi, J.D., Patchett, J.P., Ducea, M.N., Gehrels, G.E., Cecil, M.R., Rusmore, M.E., Woodsworth, G.J., Pearson, D.M., Manthei, C., and Wetmore, P., 2012, Elemental and isotopic evidence for granitoid genesis from deep-seated sources in the Coast Mountains batholith, British Columbia: Journal of Petrology, v. 53, p. 1505–1536, https://doi.org/10.1093/petrology/egs024.

Green, T.H., 1972, Crystallization of calc-alkaline andesite under controlled high-pressure conditions: Contributions to Mineralogy and Petrology, v. 34, p. 150–166, https://doi.org/10.1007/BF00373770.

Green, T.H., and Ringwood, A.E., 1968, Genesis of the calc-alkaline igneous rock suite: Contributions to Mineralogy and Petrology, v. 18, p. 105–162, https://doi.org/10.1007/BF00371806.

Greene, A.R., DeBari, S.M., Kelemen, P.B., Blusztajn, J., and Clift, P.D., 2006, A detailed geochemical study of island arc crust: The Talkeetna arc section, south-central Alaska: Journal of Petrology, v. 47, p. 1051–1093, https://doi.org/10.1093/petrology/egl002.

Hacker, B.R., Kelemen, P.B., and Behn, M.D., 2011, Differentiation of the continental crust by relamination: Earth and Planetary Science Letters, v. 307, p. 501–516, https://doi.org/10.1016/j.epsl.2011.05.024.

Hanchar, J.M., Miller, C.F., Wooden, J.L., Bennett, V.C., and Staude, J.-M.G., 1994, Evidence from xenoliths for a dynamic lower crust, eastern Mojave Desert, California: Journal of Petrology, v. 35, p. 1377–1415, https://doi.org/10.1093/petrology/35.5.1377.

Haugerud, R.A., Van der Heyden, P., Tabor, R.W., Stacey, J.S., and Zartman, R.E., 1991, Late Cretaceous and Early Tertiary plutonism and deformation in the Skagit gneiss complex, North Cascade Range, Washington and British Columbia: Geological Society of America Bulletin, v. 103, p. 1297–1307, https://doi.org/10.1130/0016-7606(1991)103<1297:LCAETP>2.3.CO;2.

Hildreth, W., and Moorbath, S., 1988, Crustal contributions to arc magmatism in the Andes of Central Chile: Contributions to Mineralogy and Petrology, v. 98, p. 455–489, https://doi.org/10.1007/BF00372365.

Hopson, C.A., and Mattinson, J.M., 1994, Chelan migmatite complex, Washington: Field evidence for mafic magmatism, crustal anatexis, mixing and protodiapiric emplacement, *in* Swanson, D.A., and Haugerud, R.A., eds., Geologic Field Trips in the Pacific Northwest: Seattle, Department of Geological Sciences, University of Washington, 1994 Geological Society of America Annual Meeting, p. 2K1–2K21.

Hurlow, H.A., and Nelson, B.K., 1993, U-Pb zircon and monazite ages for the Okanogan Range batholith, Washington: Implications for the magmatic and tectonic evolution of the southern Canadian and northern United States Cordillera: Geological Society of America Bulletin, v. 105, p. 231–240, https://doi.org/10.1130/0016-7606(1993)105<0231:UPZAMA>2.3.CO;2.

Jagoutz, O., and Schmidt, M.W., 2013, The composition of the foundered complement to the continental crust and re-evaluation of fluxes in arcs: Earth and Planetary Science Letters, v. 371–372, p. 177–190, https://doi.org/10.1016/j.epsl.2013.03.051.

Jagoutz, O.E., Burg, J.-P., Hussain, S., Dawood, H., Pettke, T., Iizuka, T., and Maruyama, S., 2009, Construction of the granitoid crust of an island arc part I: Geochronological and geochemical constraints from the plutonic Kohistan (NW Pakistan): Contributions to Mineralogy and Petrology, v. 158, p. 739–755, https://doi.org/10.1007/s00410-009-0408-3.

Jarvis, K.E., 1988, Inductively coupled plasma mass spectrometry: A new technique for the rapid or ultra-trace level determination of the rare-earth elements in geological materials: Chemical Geology, v. 68, p. 31–39, https://doi.org/10.1016/0009-2541(88)90084-8.

Johnson, D.M., Hooper, P.M., and Conrey, R.M., 1999, XRF analysis of rocks and minerals for major and trace elements on a single low dilution Li-tetraborate fused bead: Advances in X-Ray Analysis, v. 41, p. 843–867.

Karlstrom, L., Lee, C.-T.A., and Manga, M., 2014, The role of magmatically driven lithospheric thickening on arc front migration: Geochemistry Geophysics Geosystems, v. 15, p. 2655–2675, https://doi.org/10.1002/2014GC005355.

Kelemen, P.B., Hangøj, K., and Greene, A.R., 2003, One view of the geochemistry of subduction-related magmatic arcs, with an emphasis on primitive andesite and lower crust, *in* Rudnick, R., et al., eds., Treaties on Geochemistry Volume 3: New York, Elsevier, p. 593–659.

Lackey, J.S., Valley, J.W., and Saleeby, J.B., 2005, Supracrustal input to magmas in the deep crust of Sierra Nevada batholith: Evidence from high-$\delta^{18}O$ zircon: Earth and Planetary Science Letters, v. 235, p. 315–330, https://doi.org/10.1016/j.epsl.2005.04.003.

Lee, C.-T.A., Cheng, X., and Horodyskyj, U., 2006, The development and refinement of continental arcs by primary basaltic magmatism, garnet pyroxenite accumulation, basaltic recharge and delamination: Insights from the Sierra Nevada, California: Contributions to Mineralogy and Petrology, v. 151, p. 222–242, https://doi.org/10.1007/s00410-005-0056-1.

Lichte, F.E., Meier, A.L., and Crock, J.G., 1987, Determination of rare-earth elements in geological materials by inductively coupled plasma mass spectrometry: Analytical Chemistry, v. 59, p. 1150–1157, https://doi.org/10.1021/ac00135a018.

Longerich, H.P., Jenner, G.A., Fryer, B.J., and Jackson, S.E., 1990, Inductively coupled plasma–mass spectrometric analysis of geological samples: A critical evaluation based on case studies: Chemical Geology, v. 83, p. 105–118, https://doi.org/10.1016/0009-2541(90)90143-U.

Macpherson, C.G., Dreher, S.T., and Thirlwall, M.F., 2006, Adakites without slab melting: High pressure differentiation of island arc magma, Mindanao, the Philippines: Earth and Planetary Science Letters, v. 243, p. 581–593, https://doi.org/10.1016/j.epsl.2005.12.034.

Magloughlin, J.F., 1986, Metamorphic Petrology, Structural History, Geochronology, Tectonics and Geothermometry/Geobarometry in the Wenatchee Ridge Area, North Cascades, Washington [M.S. thesis]: Seattle, Washington, University of Washington, 343 p.

Mamani, M., Worner, G., and Smepere, T., 2010, Geochemical variations in igneous rocks of the Central Andean orocline (13°S to 18°S): Tracing crustal thickening and magma generation through time and space: Geological Society of America Bulletin, v. 122, p. 162–182, https://doi.org/10.1130/B26538.1.

Mattinson, C.G., Mattinson, J.M., Rioux, M., and Hopson, C.A., 2014, An ~30 million year history of mafic magmatism and partial melting in the Chelan migmatite complex, North Cascade Range, Washington, USA: Geological Society of America Abstracts with Programs, v. 46, no. 6, p. 33.

Mattinson, J.M., 1972, Ages of zircons from the Northern Cascade Mountains, Washington: Geological Society of America Bulletin, v. 83, p. 3769–3784, https://doi.org/10.1130/0016-7606(1972)83[3769:AOZFTN]2.0.CO;2.

Matzel, J.E.P., 2004, Rates of Tectonic and Magmatic Processes in the North Cascades Continental Magmatic Arc [Ph.D. thesis]: Cambridge, Massachusetts, Massachusetts Institute of Technology, 249 p.

Matzel, J.E.P., Bowring, S.A., and Miller, R.B., 2006, Time scales of pluton construction at differing crustal levels: Examples from the Mount Stuart and Tenpeak intrusions, North Cascades, Washington: Geological Society of America Bulletin, v. 118, p. 1412–1430, https://doi.org/10.1130/B25923.1.

Matzel, J.E.P., Bowring, S.A., and Miller, R.B., 2008, Spatial and temporal variations in Nd isotopic signatures across the crystalline core of the North Cascades, Washington, *in* Wright, J.E., and Shervais, J.W., eds., Ophiolites, Arcs, and Batholiths: A Tribute to Cliff Hopson: Geological Society of America Special Paper 438, p. 499–516, https://doi.org/10.1130/2008.2438(18).

Miller, R.B., 1985, The ophiolitic Ingalls complex, north-central Cascade Mountains, Washington: Geological Society of America Bulletin, v. 96, p. 27–42, https://doi.org/10.1130/0016-7606(1985)96<27:TOICNC>2.0.CO;2.

Miller, R.B., 1994, A mid-crustal contractional stepover zone in a major strike-slip system, North Cascades, Washington: Journal of Structural Geology, v. 16, p. 47–60, https://doi.org/10.1016/0191-8141(94)90017-5.

Miller, R.B., and Bowring, S.A., 1990, Structure and chronology of the Oval Peak batholith and adjacent rocks: Implications for the Ross Lake fault zone, North Cascades, Washington: Geological Society of America Bulletin, v. 102, p. 1361–1377, https://doi.org/10.1130/0016-7606(1990)102<1361.

Miller, R.B., and Paterson, S.R., 1999, In defense of magmatic diapirs: Journal of Structural Geology, v. 21, p. 1161–1173, https://doi.org/10.1016/S0191-8141(99)00033-4.

Miller, R.B., and Paterson, S.R., 2001, Construction of mid-crustal sheeted plutons: Examples from the North Cascades, Washington: Geological Society of America Bulletin, v. 113, p. 1423–1442, https://doi.org/10.1130/0016-7606(2001)113<1423:COMCSP>2.0.CO;2.

Miller, R.B., and Snoke, A.W., eds., 2009, Crustal Cross Sections from the Western North American Cordillera and Elsewhere: Implications for Tectonic and Petrologic Processes: Geological Society of America Special Paper 456, 286 p., https://doi.org/10.1130/2009.2456.

Miller, R.B., Brown, E.H., McShane, D.P., and Whitney, D.L., 1993, Intra-arc crustal loading and its tectonic implications, North Cascades crystalline core, Washington and British Columbia: Geology, v. 21, p. 255–258, https://doi.org/10.1130/0091-7613(1993)021<0255:IACLAI>2.3.CO;2.

Miller, R.B., Paterson, S.R., Lebit, H., Alsleben, H., and Lüneburg, C., 2006, Significance of composite lineations in the mid- to deep crust: A case study from the North Cascades, Washington: Journal of Structural Geology, v. 28, p. 302–322, https://doi.org/10.1016/j.jsg.2005.11.003.

Miller, R.B., Paterson, S.R., and Matzel, J.P., 2009, Plutonism at different crustal levels: Insights from the ~5–40 km (paleodepth) North Cascades crustal section, Washington, *in* Miller, R.B., and Snoke, A.W., eds., Crustal Cross Sections from the Western North American Cordillera and Elsewhere: Implications for Tectonic and Petrologic Processes: Geological Society of America Special Paper 456, p. 125–149, https://doi.org/10.1130/2009.2456(05).

Miller, R.B., Gordon, S.M., Bowring, S., Doran, B., McLean, N., Michels, Z., Shea, E., and Whitney, D.L., 2016, Linking deep and shallow crustal processes during regional transtension in an exhumed continental arc, North Cascades, northwestern Cordillera (USA): Geosphere, v. 12, p. 900–924, https://doi.org/10.1130/GES01262.1.

Miller, R.B., DeBari, S.M., and Paterson, S.R., 2018, Construction, emplacement, and geochemical evolution of deep-crustal intrusions: Tenpeak and Dirtyface plutons, North Cascades, western North America: Geosphere, v. 14, no. 3, p. 1298–1323, https://doi.org/10.1130/GES01490.1.

Misch, P., 1966, Tectonic evolution of the northern Cascades of Washington State, *in* Gunning, H. C., ed., Tectonic history and mineral deposits of the western Cordillera: Canadian Institute of Mining and Metallurgy Special Volume 8, p. 101–148.

Miyashiro, A., 1974, Volcanic rocks series in island arcs and active continental margins: American Journal of Science, v. 274, p. 321–355, https://doi.org/10.2475/ajs.274.4.321.

Müntener, O., Kelemen, P.B., and Grove, T.L., 2001, The role of H_2O during crystallization of primitive arc magmas under uppermost mantle conditions and genesis of igneous pyroxenites: An experimental study: Contributions to Mineralogy and Petrology, v. 141, p. 643–658, https://doi.org/10.1007/s004100100266.

Parent, L., 1999, Petrology and Petrogenesis of the Cardinal Peak Pluton, North Cascades, Washington [M.S. thesis]: San Jose, California, San Jose State University, 130 p.

Paterson, S.R., and Miller, R.B., 1998, Mid-crustal magmatic sheets in the Cascades Mountains, Washington: Implications for magma ascent: Journal of Structural Geology, v. 20, p. 1345–1363, https://doi.org/10.1016/S0191-8141(98)00072-8.

Paterson, S.R., Okaya, D., Memeti, V., Economos, R., and Miller, R., 2011, Magma addition and flux calculations of incrementally constructed magma chambers in continental margin arcs: Combined field, geochronologic, and thermal modeling studies: Geosphere, v. 7, p. 1439–1468, https://doi.org/10.1130/GES00696.1.

Profeta, L., Ducea, M.N., Chapman, J.B., Paterson, S.R., Gonzales, S.M.H., Kirsch, M., Petrescu, L., and DeCelles, P.G., 2015, Quantifying crustal thickness over time in magmatic arcs: Scientific Reports, v. 5, p. 17786, https://doi.org/10.1038/srep17786.

Rubin, C.M., Saleeby, J.B., Cowan, D.S., Brandon, M.T., and McGroder, M.F., 1990, Regionally extensive mid-Cretaceous west-vergent thrust system in the northwestern Cordillera: Implications for continent-margin tectonism: Geology, v. 18, p. 276–280, https://doi.org/10.1130/0091-7613(1990)018<0276:REMCWV>2.3.CO;2.

Saleeby, J., Ducea, M., and Clemens-Knott, D., 2003, Production and loss of high-density batholithic root, southern Sierra Nevada, California: Tectonics, v. 22, 1064, https://doi.org/10.1029/2002TC001374.

Sauer, K.B., Gordon, S.M., Miller, R.B., Vervoort, J.D., and Fisher, C.M., 2017, Evolution of the Jura–Cretaceous North American Cordilleran margin: Insights from detrital-zircon U-Pb and Hf isotopes of sedimentary units of the North Cascades Range, Washington: Geosphere, v. 13, p. 2094–2118, https://doi.org/10.1130/GES01501.1.

Schmitt, A.K., 2006, Laacher See revisited: High-spatial-resolution zircon dating indicates rapid formation of a zoned magma chamber: Geology, v. 34, p. 597–600, https://doi.org/10.1130/G22533.1.

Schwartz, J.J., Johnson, K., Mueller, P., Valley, J., Strickland, A., and Wooden, J.L., 2014, Time scales and processes of Cordilleran batholith construction and high-Sr/Y magmatic pulses: Evidence from the Bald Mountain batholith, northeastern Oregon: Geosphere, v. 10, p. 1456–1481, https://doi.org/10.1130/GES01033.1.

Schwartz, J.J., Klepeis, K.A., Sadorski, J.F., Stowell, H.H., Tulloch, A.J., and Coble, M.A., 2017, The tempo of continental arc construction in the Mesozoic Median batholith, Fiordland, New Zealand: Lithosphere, v. 9, p. 343–365, https://doi.org/10.1130/L610.1.

Shand, S.J., 1943, Eruptive Rocks: Their Genesis, Composition, Classification, and Their Relations to Ore Deposits with a Chapter on Meteorites: New York, John Wiley, 444 p.

Shea, E.K., 2014, Arc Magmatism at Different Crustal Levels, North Cascades, WA [Ph.D. thesis]: Cambridge, Massachusetts, Massachusetts Institute of Technology, 547 p.

Shea, E.K., Miller, J.S., Miller, R.B., Bowring, S.A., and Sullivan, K.M., 2016, Growth and maturation of a mid- to shallow-crustal intrusive complex, North Cascades, WA: Geosphere, v. 12, p. 1489–1516, https://doi.org/10.1130/GES01290.1.

Sun, S.S., and McDonough, W.F., 1989, Chemical and isotopic systematics of oceanic basalts: Implications for mantle composition and processes, *in* Saunders, A.D., and Norry, M.J., eds., Magmatism in the Ocean Basins: Geological Society, London, Special Publication 42, p. 313–345, https://doi.org/10.1144/GSL.SP.1989.042.01.19.

Tabor, R., Haugerud, R., and Miller, R., 1989, Accreted Terranes of the North Cascades Range, Washington: Washington, D.C., American Geophysical Union, International Geological Congress Trip T307, 62 p.

Valley, J.W., 2003, Oxygen isotopes in zircon, *in* Hanchar, J.M., and Hoskin, P.W.O., eds., Zircon: Mineralogical Society of America Reviews in Mineralogy and Geochemistry 53, p. 343–385.

Valley, P.M., Whitney, D.L., Paterson, S.R., Miller, R.B., and Alsleben, H., 2003, Metamorphism of the deepest exposed arc rocks in the Cretaceous to Paleogene Cascades belt, Washington: Evidence for large-scale vertical motion in a continental arc: Journal of Metamorphic Geology, v. 21, p. 203–220, https://doi.org/10.1046/j.1525-1314.2003.00437.x.

VanDiver, B.B., 1967, Contemporaneous faulting-metamorphism in Wenatchee Ridge area, North Cascades, Washington: American Journal of Science, v. 265, p. 132–150, https://doi.org/10.2475/ajs.265.2.132.

Vervoort, J.D., and Blichert-Toft, J., 1999, Evolution of the depleted mantle: Hf isotope evidence from juvenile rocks through time: Geochimica et Cosmochimica Acta, v. 63, p. 533–556, https://doi.org/10.1016/S0016-7037(98)00274-9.

Whitney, D.L., Miller, R.B., and Paterson, S.R., 1999, *P-T-t* evidence for mechanisms of vertical tectonic motion in a contractional orogen: Northwestern US and Canadian Cordillera: Journal of Metamorphic Geology, v. 17, p. 75–90, https://doi.org/10.1046/j.1525-1314.1999.00181.x.

Zen, E-an, 1988, Tectonic significance of high-pressure plutonic rocks in the western Cordillera of North America, *in* Ernst, W.G., ed., Metamorphic and Crustal Evolution of the Western United States—Rubey Volume VII: Englewood Cliffs, New Jersey, Prentice Hall, p. 41–67.

MANUSCRIPT RECEIVED 18 APRIL 2018
REVISED MANUSCRIPT RECEIVED 21 JULY 2018
MANUSCRIPT ACCEPTED 6 SEPTEMBER 2018